

# Quasiconformal Mappings with Surface Domains

ANTHONY GRUBER, Florida State University  
EUGENIO AULISA, Texas Tech University

Quasiconformal mappings from surfaces immersed in Euclidean space are discussed for the purposes of computing dilatation-optimal surface meshes with prescribed connectivity and Dirichlet boundary data. In particular, a quaternionic formulation of quasiconformality is proposed which leads to a linear algorithm for computing least-squares quasiconformal maps from surfaces given as extrinsic mesh data. This facilitates an iterative procedure which computes optimal quasiconformal mappings with optional constraints on surface area and extrinsic geometry. Based on the established Quasiconformal Iteration method, the proposed algorithm produces high quality surface mappings which correctly capture boundary information while eliminating undesirable folds which appear during least-squares conformal mapping procedures.

CCS Concepts: • Computing methodologies → Shape modeling; • Mathematics of computing → Partial differential equations.

Additional Key Words and Phrases: quasiconformal mapping, Teichmüller mapping, mesh optimization, surface remeshing

## ACM Reference Format:

Anthony Gruber and Eugenio Aulisa. 2022. Quasiconformal Mappings with Surface Domains. *ACM Trans. Graph.* 37, 4, Article 111 (June 2022), 22 pages.  
<https://doi.org/10.1145/nnnnnnn.nnnnnnn>

## 1 INTRODUCTION

Conformal maps between two-dimensional Riemann surfaces are widely recognized as useful tools in both theoretical and computational settings, as enough interesting quantities are conformally invariant (e.g. the total Gaussian curvature and the Willmore energy of surfaces) that many difficult problems can be made considerably simpler by applying an appropriate conformal transformation. Indeed, at the present time there are several effective algorithms for computing conformal or nearly conformal mappings (see e.g. [Bobenko et al. 2015; Gu et al. 2004; Gu and Yau 2003; Kharevych et al. 2006; Sawhney and Crane 2017; Springborn et al. 2008; Trefethen 2020] and references therein), the use cases of which cover everything from surface flattening to medical image registration. Despite this, it is also well known that conformal maps are unsuitable for mapping problems with a pointwise boundary correspondence, and there is very often no conformal map between two connected surfaces which maps boundaries to boundaries in a prescribed way even in quite simple cases. For example, it can be shown that there

---

Authors' addresses: Anthony Gruber, agruber@fsu.edu, Florida State University, 600 W College Ave, Tallahassee, Florida, 32306; Eugenio Aulisa, eugenio.aulisa@ttu.edu, Texas Tech University, P.O. Box 41042, Lubbock, Texas, 79409.

---

Permission to make digital or hard copies of all or part of this work for personal or classroom use is granted without fee provided that copies are not made or distributed for profit or commercial advantage and that copies bear this notice and the full citation on the first page. Copyrights for components of this work owned by others than ACM must be honored. Abstracting with credit is permitted. To copy otherwise, or republish, to post on servers or to redistribute to lists, requires prior specific permission and/or a fee. Request permissions from [permissions@acm.org](mailto:permissions@acm.org).

© 2022 Association for Computing Machinery.  
0730-0301/2022/6-ART111 \$15.00  
<https://doi.org/10.1145/nnnnnnn.nnnnnnn>

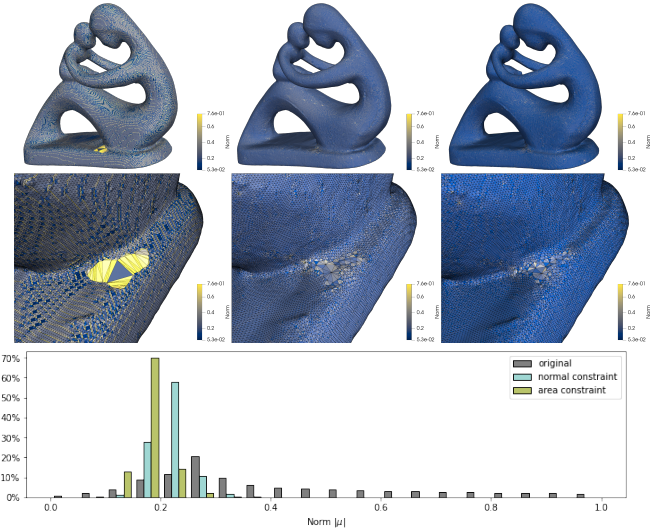


Fig. 1. Quasiconformal remeshings (c.f. Section 6.2) of a statue mesh with genus four constructed using the QC Iteration algorithm from Section 5 with reference conformal structure constructed using Algorithm 5. Left: original surface; Middle: remeshing with normal constraint (c.f. Section 4.1). Right: remeshing with area constraint (c.f. Section 4.2). Bottom: histogram of the norm of the Beltrami coefficient  $\mu$ .

is no corner-preserving conformal mapping from a square onto a rectangle; no matter the ratio of lengths, there is an inevitable amount of shearing distortion that occurs during this process which is inherently non-conformal. This presents a significant challenge for computational applications which involve some form of mesh deformation, where a conformal (or close-to-conformal) mapping is desired which satisfies some given boundary data. While least-squares conformal mapping techniques can certainly be applied in this instance, they are known to produce undesirable folds if the target surface is non-convex (see e.g. Figure 2 or Figure 5).

On the other hand, in many cases it is sufficient to relax the condition of conformality to include the possibility of uniformly bounded shearing distortion. These mappings are known as quasiconformal, and they are relatively abundant by comparison with their conformal analogues. In fact, a mild growth condition on the distortion at the boundary guarantees the existence and uniqueness of a “best possible” quasiconformal map between two Riemann surfaces (c.f. Theorem 2.2) in a given homotopy class. Known as a Teichmüller mapping, this extremal object minimizes the maximal conformality distortion in this class, producing an exceptionally regular object useful for a multitude of tasks in areas such as image processing, object deformation, and surface registration.

### 1.1 Related Work

Due to their advantageous properties, quasiconformal (QC) mappings have recently been investigated for a variety of computational applications. This usually involves manipulating some form of the Beltrami equation  $f_z = \mu f_z$  (see Section 2), which characterizes quasiconformality and can be discretized and solved on constructions such as a manifold mesh or point cloud. In particular, planar quasiconformal mappings are used in [Zeng and Gu 2011] for surface registration by pre-composing the computation of the Beltrami coefficient (BC)  $\mu$  with a Ricci flow procedure to homogenize the domain. Similarly, [Zeng et al. 2012] employ a discrete version of the Yamabe flow to compute planar Teichmüller mappings by evolving a given quasiconformal metric to a Teichmüller minimum, and [Ng et al. 2014] employ a perturbative “Beltrami holomorphic flow” to the same effect. In a different direction, [Lipman 2012] formulates convex spaces of bounded distortion mappings which are computable and contain quasiconformal mappings as a subclass, while [Nian and Chen 2016] uses B-spline techniques to compute quasiconformal mappings for isogeometric analysis. The authors of [Weber et al. 2012] make use of holomorphic quadratic differentials to formulate a minimization-based method for computing extremal Teichmüller maps between planar domains with boundary, or genus 0 surfaces with additional conformal mapping. Yet another approach is taken in [Lui et al. 2014] where an alternating minimization called the “QC Iteration” is developed for computing Teichmüller mappings of planar domains and genus 0 surfaces. This QC iteration is connected to the theory of harmonic mappings in [Lui et al. 2015] and shown to converge under some assumptions. More recently, works such as [Choi 2021] have also attempted to connect quasiconformality back to conformality by using quasiconformal mappings as a way to obtain nearly-conformal parameterizations of planar domains.

Besides those methods discussed so far involving planar manifold meshes, the available techniques for computing quasiconformal maps have since been expanded to include other topological types as well as other forms of data. The work [Meng et al. 2016] develops an algorithm called TEMPO for computing Teichmüller mappings on point clouds. Moreover, quasiconformal maps of multiply-connected planar domains with prescribed distortion are computed in [Ho and Lui 2016], and [Lee et al. 2016] compute quasiconformal maps between 3D volumes for the purpose of surface registration. The variety of algorithms available for computing quasiconformal maps has also led to a number of interesting applications, such as a quasiconformal kernel for nearest neighbor calculations in machine learning algorithms [Peng et al. 2004] as well as a method for feature-preserving image resizing [Xu et al. 2018]. In addition, quasiconformal mappings have also been used to create origami-like surfaces with prescribed folds [Qiu et al. 2019], to compute quasiconformal rectilinear mappings for planar subdivision surfaces [Yang and Zeng 2020], and even to study the morphometry of human teeth [Choi et al. 2020].

### 1.2 Contributions

Despite the far-reaching interest into quasiconformal mappings and their applications, at present there are no methods which are adequate for computing quasiconformal mappings between surfaces

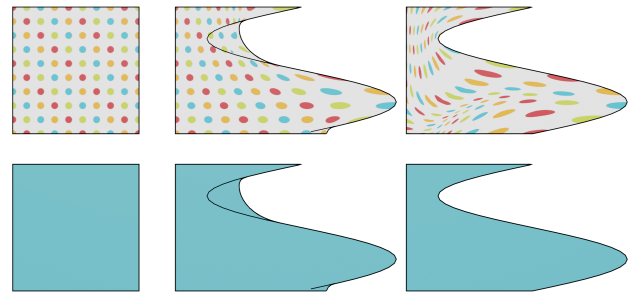


Fig. 2. Comparison between least-squares conformal mapping (LSCM, middle) and Teichmüller quasiconformal mapping (TQCM, right) on a planar domain with boundary. Note that the least-squares conformal mapping does not respect injectivity, despite producing less average texture distortion.

of nonzero genus. While several of the methods mentioned in Section 1.1 can conceivably be applied piece-wise after e.g. cutting each surface along the generators of its fundamental group, it is a nontrivial matter in practice to compose such a procedure with the quasiconformal mapping algorithms above. Even more surprisingly, there appear to be no algorithms yet in place for computing quasiconformal mappings directly from a non-planar surface of any genus. Instead, non-planar domains must first be mapped conformally to the plane, which is often nontrivial and requires additional computational resources.

The present work addresses these issues in the case that the source surface is embedded (or more generally, immersed) in  $\mathbb{R}^3$  by providing a direct algorithm for computing quasiconformal mappings with prescribed Dirichlet boundary conditions, which can be applied to surfaces of arbitrary genus. Using a discretization based on finite elements, this procedure is essentially a single linear solve which computes a least-squares quasiconformal mapping with respect to some predefined BC  $\mu$  given as a value-per-polygon. It is shown that the present algorithm for computing quasiconformal maps enables an extension of the useful Quasiconformal Iteration algorithm of Lui et al. [Lui et al. 2014] mentioned previously, which computes the extremal Teichmüller map  $f : M \rightarrow P$  between two connected planar domains, or (with additional conformal mapping) between two connected, genus zero Riemann surfaces with boundary. The technology introduced here extends the applicability of the QC Iteration to maps from surfaces of arbitrary genus which are represented as (planar or non-planar) manifold meshes in  $\mathbb{R}^3$ , giving a useful procedure for folding-free object deformation and surface remeshing. Specifically, the present contributions are:

- An intrinsic-to-extrinsic formulation of quasiconformal mappings  $f : M \rightarrow f(M) \subset \mathbb{R}^3$  based on quaternionic theory which is convenient for computation.
- A self-contained, genus-agnostic algorithm for computing quasiconformal mappings whose domain is a manifold mesh in  $\mathbb{R}^3$ .
- An extension of the QC Iteration algorithm for computing Teichmüller mappings to this setting, which approximates

optimal Teichmüller mappings from immersed surfaces which are simply connected and dilatation-uniform quasiconformal mappings otherwise.

- Applications to surface remeshing and the construction of locally injective mappings satisfying prescribed Dirichlet boundary conditions.

The remainder of this work is structured as follows. The basics of quasiconformal maps and the QC Iteration are presented in Section 2. Section 3 gives the novel quaternionic formulation of quasiconformality which enables the main algorithm in Section 4. Section 5 then extends the QC Iteration to the present setting, and some numerical applications of this are discussed in Section 6.

## 2 PRELIMINARIES

This Section recalls the standard presentation of extremal quasiconformal mappings which is necessary to describe the QC Iteration algorithm of [Lui et al. 2015, 2014]. More information regarding the theory of quasiconformal mappings can be found in [Gardiner and Lakic 2000; Hubbard 2006; Strebel 1984], and a good account of the connection between Teichmüller and harmonic mappings is given in [Daskalopoulos and Wentworth 2007].

### 2.1 Extremal Quasiconformal Mappings

Recall that a quasiconformal map  $f : M \rightarrow P$  between Riemann surfaces is an orientation-preserving homeomorphism which has bounded conformality distortion with respect to a given (almost) complex structure  $J$  on  $TM$ . In standard notation (c.f. [Hubbard 2006, Section 4.8]),  $f$  is  $\mu$ -quasiconformal provided it satisfies the *Beltrami equation*,

$$\bar{\partial}f = \partial f \circ \mu,$$

where  $\partial, \bar{\partial}$  are the  $\mathbb{C}$ -linear resp.  $\mathbb{C}$ -antilinear parts of the natural derivative operator  $df : TM \rightarrow TP$  and  $\mu : TM \rightarrow TM$ ,  $|\mu|_\infty < 1$ , is the  $\mathbb{C}$ -antilinear *Beltrami coefficient* (also called Beltrami differential and abbreviated BC) of the mapping. In a local conformal coordinate  $z : U \subset M \rightarrow \mathbb{C}$ , this implies the expression

$$f_z = \mu f_{\bar{z}},$$

where  $f_z := \partial_z f$  (resp.  $f_{\bar{z}} := \partial_{\bar{z}} f$ ) are the partial derivatives of the mapping  $f$  with respect to the conformal coordinate  $z$  and  $\mu : U \rightarrow \mathbb{C}$  is the locally defined BC. Notice that  $f$  is conformal if and only if  $\mu \equiv 0$ , and this condition depends only on the conformal structure of  $M$ .

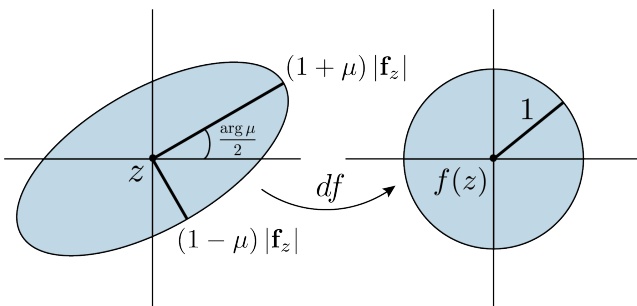


Fig. 3. The geometry of a quasiconformal mapping  $f : M \rightarrow \mathbb{R}^3$ .

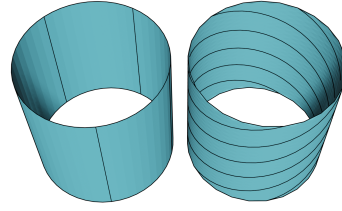


Fig. 4. Two non-homotopic families of maps from an interval to the cylinder (i.e. curves) with identical boundary data.

Geometrically, the Beltrami equation implies that quasiconformal maps take small circles on the source space to small ellipses of bounded eccentricity on the target (see Figure 3). To see this, suppose  $f : M \rightarrow f(M) \subset \mathbb{R}^3$  immerses the surface  $M$  in Euclidean space. Let  $g$  be a Riemannian metric on  $M$  with local expression  $g = \sigma |dz|^2$  for some positive function  $\sigma : U \rightarrow \mathbb{R}$ , and denote the Euclidean metric on  $\mathbb{R}^3$  by  $\delta$ . Then, the Jacobian determinant describing the local area distortion of  $f$  has the expression

$$\text{Jac}(f) = |f_z|^2 - |f_{\bar{z}}|^2 = |f_z|^2 \left(1 - |\mu|^2\right) = \sqrt{\lambda_1 \lambda_2},$$

where  $\lambda_1, \lambda_2$  are the eigenvalues of the pullback metric  $f^*\delta$  on  $M$  relative to the flat metric  $|dz|^2$ . Moreover, since

$$f^*\delta = \langle df, df \rangle = |f_z|^2 |dz + \mu d\bar{z}|^2,$$

these eigenvalues are given by

$$\lambda_1 = |f_z|^2 (1 + |\mu|)^2, \quad \lambda_2 = |f_z|^2 (1 - |\mu|)^2.$$

These are the squared lengths of the major resp. minor axes of the ellipse in  $T_z M$  which pushes forward under  $df$  to the unit circle in  $T_{f(z)} f(M)$ , quantifying the shearing distortion induced by quasiconformality. Their ratio defines the maximal dilatation of  $f$ ,

$$K(f) = \frac{1 + |\mu|_\infty}{1 - |\mu|_\infty},$$

which is  $1 \leq K < \infty$  for orientation-preserving maps and  $-\infty < K < -1$  for orientation-reversing maps. Note that  $\text{Jac}(f) > 0$  when  $f_z \neq 0$  and  $|\mu| < 1$ , reflecting the remarkable fact that quasiconformal mappings are locally injective. In the discrete setting, this implies that  $f$  cannot have fold-overs or wrap-ups (i.e. places where the mapping fails to be immersive, see Figures 2, 5, and 13), which is essential in applications such as medical device simulations where surfaces must remain embedded as they deform.

Although there are generally many quasiconformal mappings from one Riemann surface to another, there are relatively few which are distinguished as being extremal. These are the mappings  $f$  which minimize the maximal dilatation  $K$ , i.e.

$$K(f) \leq K(f'),$$

for any map  $f' : M \rightarrow P$  homotopic to  $f$  (denoted  $f' \sim f$ ) relative to the boundary  $\partial M$  (see Figure 4 for an illustration). Such maps always exist for each homotopy class,

$$[f] = \{f' : M \rightarrow P : f'|_{\partial M} = f|_{\partial M} \text{ and } f' \sim f\}$$

but need not be unique. On the other hand, in many circumstances there is a unique extremal map of special form which is compatible with the given boundary data. This is called a Teichmüller map,

and has the desirable property of uniform conformality distortion throughout the whole domain.

**Definition 2.1.** The quasiconformal mapping  $f : M \rightarrow f(M)$  between Riemann surfaces is said to be *Teichmüller* provided there exists a constant  $0 < k < 1$  and holomorphic quadratic differential  $q \in T^*M \otimes T^*M$  such that in any local conformal coordinate  $z : U \subset M \rightarrow \mathbb{C}$  the Beltrami coefficient  $\mu : TM \rightarrow TM$ ,  $\mu = \mu(z)d\bar{z} \otimes \frac{\partial}{\partial z}$  satisfies

$$\mu(z) = k \frac{\bar{q}(z)}{|q(z)|}, \quad k = \|q\|_1 = \int_M |q|,$$

where  $q = q(z)dz^2$ . In this case,  $\mu$  is said to be Teichmüller associated to  $f$ .

It is a fact that when a Teichmüller map exists, it is unique and extremal for its homotopy class. Moreover, existence is guaranteed in many practically-relevant situations thanks to classical results in complex analysis. In particular, define the boundary dilatation of the homotopy class  $[f]$  as

$$H([f]) = \inf_{f' \in [f]} \left\{ \inf_{C \subset M} K(f'|_{M \setminus C}) \right\},$$

where  $C$  is any compact set strictly contained in  $M$ . The primary existence result for Teichmüller maps in terms of this criterion is due to Strebel [Strebel 1984].

**THEOREM 2.2.** [Gardiner 1987, Theorem 9, Section 6.8] Let  $M$  be a connected Riemann surface with potential boundary, and let  $f : M \rightarrow f(M)$  be quasiconformal. Suppose the boundary dilatation  $H([f]) < K(f)$ . Then,  $[f]$  contains a unique extremal Teichmüller mapping with Beltrami coefficient  $\mu = k\bar{q}/|q|$  for a unique constant  $0 < k < 1$  and a quadratic differential  $q \in T^*M \otimes T^*M$  which is integrable, holomorphic, and unique up to multiplication by a positive constant.

**Remark 2.3.** Note that the Teichmüller mappings from [Strebel 1978, Theorem 8] are allowed to correspond to quadratic differentials which are meromorphic with at most one simple pole, as opposed to purely holomorphic. This definition considerably widens the space of Teichmüller maps, at the cost of uniqueness in certain settings. Practically, QC Iteration may produce mappings with this same structure, see e.g. the simple pole on the front of the surface in Figure 9, which is also visible in the lower-right image of Figure 5.

## 2.2 Quasiconformal remeshing

From Theorem 2.2 and the above discussion, it is clear that Teichmüller maps are remarkably well-behaved. In particular, any quasiconformal map  $f : M \rightarrow P$  between Riemann surfaces satisfying “nice enough” boundary conditions contains a unique Teichmüller extremal map in its homotopy class. Conversely, it turns out that even when no extremal Teichmüller map exists, there is always a Teichmüller map with dilatation arbitrarily close to the extremal one (see [Strebel 1978, Theorem 8]). In some sense, this makes Teichmüller maps the best possible quasiconformal mappings between Riemann surfaces  $M$  and  $P$ , and this property has encouraged their use in computational applications such as folding-free object deformation (as in Figures 2, 5) and computational remeshing (as in Figure 1). While these applications are discussed at length in

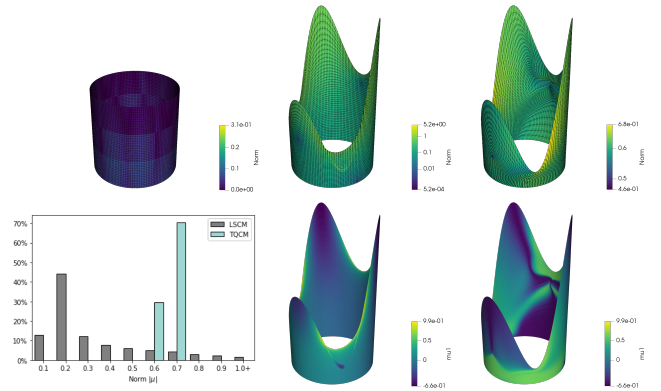


Fig. 5. Comparison of LSCM (mid) and TQCM (right) on a cylinder with prescribed boundary; top row colored by  $|\mu|$  and bottom row colored by the first component  $\mu^1$ . Similar to the planar case, LSCM creates undesirable spillage and cannot guarantee injectivity. Conversely, TQCM remains injective despite a height distortion of 80% at the boundary. Note the visible discontinuities in  $\mu^1$  as expected (c.f. Figure 9).

Section 6, it is worth mentioning explicitly how quasiconformal mappings are useful for surface remeshing in order to understand some of the Figures which appear in the meantime. To that end, consider an immersed surface  $M \subset \mathbb{R}^n$  ( $n = 2, 3$ ) presented in discrete form as a list of vertex positions in  $\mathbb{R}^n$  along with an associated polygon mesh defining its connectivity. Then, the discrete surface (also called  $M$ ) inherits a Riemannian metric  $g$  which comes from restricting the Euclidean inner product to each polygon, which in turn defines a discrete conformal structure on  $M$  determined by the interior angles of these polygons. Now, it is often the case in practice that many of these angles are nearly degenerate (see e.g. Figure 1, left column), leading to a substantial amount of discretization error which appears “downstream” when e.g. differential equations are solved on  $M$ . To alleviate this, it is standard to look for a different discretization of  $M$  with a more regular discrete conformal structure, so that a “better” triangulation of the surface can be obtained from a preprocessing step. Notably, one way to accomplish this is with an appropriate quasiconformal mapping  $f : (M, g_{\text{ref}}) \rightarrow (M, g)$  where  $g_{\text{ref}}$  is a pre-supplied reference metric belonging to the desired conformal class  $[g_{\text{ref}}]$ ; in this way, the original discrete surface  $M$  is suitably remeshed through a direct application of the mapping  $f$ . Moreover, with this approach it is enough to specify  $[g_{\text{ref}}]$  through a simple list of target interior angles (c.f. Section 6.2), since the notion of quasiconformality does not depend on any particular metric representative. This is precisely what enables the remeshing applications seen in this work, which are facilitated by the quaternionic formulation in Section 3 as well as the QC Iteration algorithm of [Lui et al. 2015, 2014].

## 2.3 The Quasiconformal (QC) Iteration

The Quasiconformal (QC) Iteration algorithm introduced in [Lui et al. 2014] is an approach to computing extremal Teichmüller mappings between planar domains and between surfaces which are conformal to planar domains. Its general idea is to find a downward

trajectory toward the optimal Teichmüller map in a given homotopy class by alternately minimizing the distortion induced by a particular BC  $\mu$  and the deviation of  $\mu$  from Teichmüller form as defined in Definition 2.1. Under the somewhat restrictive assumptions mentioned in [Lui et al. 2015] (such as nonpositive Gaussian curvature of the target), this algorithm is guaranteed to converge to a unique Teichmüller mapping between simply or multiply connected Riemann surfaces of the same topology. In fact, the QC Iteration typically exhibits good practical performance even in cases when a unique Teichmüller extremum cannot be guaranteed, converging to a mapping with near-constant dilatation in many cases of interest regardless of these assumptions. The goal of this Subsection is to recall some details of the QC Iteration algorithm which will be necessary for its extension to general immersed surfaces in Section 5.

Let  $(M, J)$  be a Riemann surface as before and choose a Riemannian metric  $g$  compatible with  $J$ . Essentially, the QC Iteration is a recipe to minimize the *quasiconformal distortion* of  $f : (M, g) \rightarrow (P, h)$  with respect to an evolving BC  $\mu$ ,

$$QC_\mu(f) = \int_M |\bar{\partial}f - \partial f \circ \mu|_h^2 dS_g,$$

where  $P$  is a target Riemann surface of the same topology equipped with Riemannian metric  $h$ ,  $|\cdot|_h$  denotes the norm with respect to  $h$ , and  $dS_g$  denotes the area element of  $(M, g)$ . Clearly,  $f : M \rightarrow P$  is quasiconformal with respect to  $\mu$  if and only if  $QC_\mu(f) = 0$ , and it is shown in Appendix A that the quasiconformal distortion of a map  $f' \in [f]$  with respect to a given  $\mu$  can be interpreted as the “conformal part” of the Dirichlet energy  $\mathcal{D}_{g(\mu)}(f')$  where  $g(\mu)$  is a canonical representative of the conformal class of metrics on  $M$  defined by  $\mu$ , i.e.  $QC_\mu$  measures precisely the amount by which the mapping  $f' : (M, g(\mu)) \rightarrow (P, h)$  fails to be conformal with respect to  $[g(\mu)]$ . In fact, it can be shown that in many cases of interest there is a unique minimizer of  $\mathcal{D}_{g(\mu)}$  for each  $\mu$ , and therefore the unique Teichmüller mapping  $f^* : (M, g) \rightarrow (P, h)$  in the homotopy class  $[f]$  can be approached by way of these minimizers. This gives an interpretation of the QC Iteration from [Lui et al. 2015] in terms of harmonic mappings which is useful for analysis and briefly explored in Appendix B.

More practically, the QC Iteration algorithm is an iterative three-stage process for jointly minimizing  $QC_\mu$  with respect to  $f$  and  $\mu$  formulated in [Lui et al. 2014] and loosely described by the following:

- (1) Fix  $\mu$  and minimize  $QC_\mu(f)$  for  $f : (M, g) \rightarrow (P, h)$ .
- (2) Compute  $\mu$  algebraically from  $f$ .
- (3) Locally post-process  $\mu$  to bring it closer to Teichmüller form.

Steps 1 and 2 of this procedure are relatively straightforward to describe for planar domains  $M \subset \mathbb{C}$  that can be covered by a single local coordinate chart  $U \supset M$  where  $g = \sigma |dz|^2$  for some positive  $\sigma : U \rightarrow \mathbb{R}$ . In this case,  $\mu : U \rightarrow \mathbb{C}$  can be interpreted as a complex-valued function and the distortion  $QC_\mu$  takes the simple expression,

$$\begin{aligned} 2QC_\mu(f) &= \int_U \frac{1}{\sigma} |\mathbf{f}_z - \mu \mathbf{f}_z|_h^2 \sigma idz \wedge d\bar{z} \\ &= \int_U |\mathbf{f}_z - \mu \mathbf{f}_z|_h^2 idz \wedge d\bar{z}, \end{aligned}$$

which can be linearized around a reference mapping, set equal to zero, and solved directly to yield  $f$  in a least-squares sense. Moreover,

the use of complex algebra to describe  $f$  and  $\mu$  means that the new  $\mu$  associated to the most recently computed  $f$  can be readily recovered as

$$\mu = \frac{\mathbf{f}_z}{\mathbf{f}_z},$$

where the vector quotient on the RHS is interpreted as the division of complex numbers. Since computations like these are no longer straightforward on general immersed Riemannian surfaces  $M \subset \mathbb{R}^3$ , a primary contribution of the present work is an extension of these ideas to more general surface data (e.g. Figure 6) in Sections 4 and 5 using ideas from quaternion algebra introduced in Section 3.

In contrast to this, Step 3 of the QC Iteration is subtle regardless of the involved geometry and represents an indirect way to move  $\mu$  toward the global Teichmüller optimum by manipulating its local structure. This is facilitated by the following fact proved for convenience in Appendix C.

**LEMMA 2.4.** *Any Teichmüller Beltrami coefficient  $\mu : TM \rightarrow TM$  has harmonic norm, as well as harmonic argument when restricted to local charts  $U \subset M$  where  $q \neq 0$ . Conversely, any pair  $(k, \theta)$  where  $k \in \mathbb{R}$  and  $\theta : U \rightarrow \mathbb{R}$  is harmonic can be associated with a Teichmüller Beltrami coefficient  $\mu$  on  $U$ .*

By this result, the BC  $\mu^*$  associated to the unique Teichmüller mapping  $f^* \in [f]$  should have constant norm and harmonic argument when restricted to any local coordinate system away from the zeros of the quadratic differential  $q$ . Therefore, Step 3 in the QC Iteration is to gently perturb the  $\mu$  computed in Step 2 so as to bring its norm to constant while roughly smoothing its argument. This involves a straightforward projection of the norm onto its average value

$$|\mu| \leftarrow \frac{\int_M |\mu| dS_g}{\int_M dS_g},$$

followed by a single step of Jacobi iteration applied to  $\arg \mu$ . This usually (although not always) results in an iterate  $\mu$  with lower “Beltrami energy” (see Appendix B for details) which is used as the input to the next iteration. Note that the smoothing Step 3 will cease to perturb the optimal  $\mu^*$  away from the zeros of  $q$  by design, since Lemma 2.4 guarantees that the norm is constant and the argument is harmonic.

**Remark 2.5.** Since the argument of the BC  $\mu$  is only well defined away from the zeros of the quadratic differential  $q$ , so is the smoothing procedure proposed in [Lui et al. 2014]. For this reason, the extended algorithm presented in Section 5 smooths on the phase  $e^{i \arg \mu} = \mu / |\mu|$  which is well defined everywhere on  $M$  but not continuous, as can be seen in e.g. Figure 5 (bottom right). Since  $\Delta e^{i \arg \mu} = e^{i \arg \mu} (i \Delta \arg \mu - |\nabla \arg \mu|^2)$ , these procedures are equivalent when  $M$  is simply connected.

While quasiconformal mappings remain important tools for computational tasks such as meshing and surface registration, their present utility is limited by the use of planar technology such as what has just been described. Computing quasiconformal mappings between generic Riemann surfaces in this way requires sophisticated pre- and post-processing with conformal flattening procedures, as



Fig. 6. Quasiconformal mapping from a simply connected surface equipped with an ideal conformal structure (c.f. Section 6.2) to itself equipped with the usual conformal structure inherited from its embedding in  $\mathbb{R}^3$ .

well as attention to highly nontrivial issues of compatibility between solutions computed on different surface patches. To develop a coordinate-free alternative to this in the case that the source surface  $M \subset \mathbb{R}^3$  is given extrinsically, The next Section discusses a formulation of quasiconformality using quaternionic surface theory which enables the direct computation of quasiconformal maps from immersed Riemann surfaces of any genus.

### 3 QUASICONFORMALITY WITH QUATERNIONS

The present approach to computing quasiconformal mappings is facilitated by technology from quaternionic surface theory, the details of which are discussed in [Burstall et al. 2004; Kamberov et al. 2002]. Recall that the quaternions  $\mathbb{H}$  are the 4-dimensional division algebra over  $\mathbb{R}$  generated by the set of symbols  $\{i, j, k\}$  satisfying the relations  $i^2 = j^2 = k^2 = ijk = -1$ . It turns out that the additional algebraic structure provided by  $\mathbb{H}$  is advantageous for studying the conformal geometry of immersed surfaces in a variety of settings. In particular, any immersion  $f : M \rightarrow \mathbb{R}^3$  of the two-dimensional surface  $M$  can be regarded as taking values in the imaginary part of the quaternions  $\text{Im } \mathbb{H} \cong \mathbb{R}^3$ , and therefore multiplication in  $\mathbb{H}$  (conventionally acting on the right) can be applied. This leads to a coordinate-free theory of surfaces which is adaptable, concise, and well suited for computational applications.

To explain the basic idea behind this, let  $(M, J)$  be a connected Riemann surface with (possibly empty) boundary  $\partial M$  and complex structure  $J : TM \rightarrow TM$  satisfying  $J^2 = -\mathbb{1}_{TM}$ . Then,  $M$  carries a natural conformal structure inherited from the scalar product on each tangent space, and an immersion  $f : (M, J) \rightarrow \mathbb{R}^3$  is conformal provided it maps oriented orthogonal bases of  $TM$  to oriented orthogonal bases of  $df(TM)$ . By standard arguments (e.g. [Burstall et al. 2004, Lemma 2]), this implies the existence of a unit quaternion field  $N : M \rightarrow S^2 \subset \text{Im } \mathbb{H}$  uniquely compatible with the orientation on  $M$  that stabilizes  $df(TM)$ , i.e. such that  $df(TM) = \{\mathbf{v} \in \text{Im } \mathbb{H} \mid N\mathbf{v}N = \mathbf{v}\}$ . It follows that  $N$  is the Gauss map of the immersion  $f$ , and moreover that  $f$  is conformal when and only when there exists an  $N : M \rightarrow S^2$  satisfying

$$*df = N df,$$

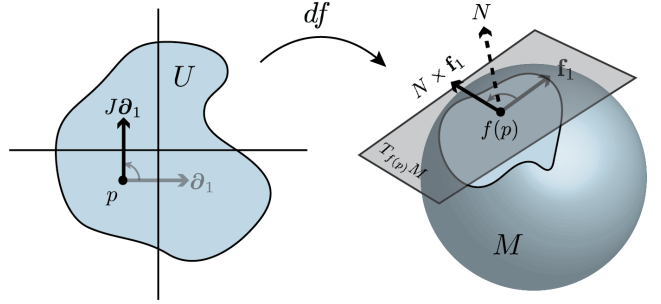


Fig. 7. An illustration of a conformal mapping  $f : M \rightarrow \text{Im } \mathbb{H} \cong \mathbb{R}^3$  localized to a patch  $U \subset M$ . Here  $f_1 := df(\partial_1)$  and  $*df(\partial_1) = df \circ J(\partial_1) = N df(\partial_1) = N \times f_1$  since  $N \perp df$ .

where  $*df := df \circ J$  is the negative Hodge star operator on differential one-forms. This provides a useful link illustrated in Figure 7 between the intrinsic notion of conformality and its extrinsic expression in terms of the surface Gauss map.

#### 3.1 A useful definition

The key to the results presented here is a description of quasiconformal mappings in terms of this quaternionic framework. First, note that the Gauss map  $N : M \rightarrow S^2$  of any conformal immersion  $f : M \rightarrow \text{Im } \mathbb{H}$  defines a canonical complex structure on  $TM$  (c.f. [Burstall et al. 2004, Section 2.1]) which conventionally acts on the left. Indeed, it is straightforward to check that the mapping  $J : TM \rightarrow TM$  defined by

$$(a + Jb)v = a df(v) + b N df(v),$$

for all  $a, b \in \mathbb{R}$  and  $v \in TM$  is a complex structure on  $TM$  compatible with  $N$ .

**Remark 3.1.** It will often be useful to “forget” about the reference immersion in the case of  $M \subset \mathbb{R}^3 \cong \text{Im } \mathbb{H}$ , regarding  $(M, J)$  as an abstract surface even when  $J$  is defined by a Gauss map  $N$  of this immersion. This allows for notational flexibilities such as  $f : M \rightarrow f(M) \subset \mathbb{R}^3$  which will be freely adopted in the remainder of the work when the context is clear. Additionally, it is interesting to note that every conformal structure  $J$  on  $TM$  can be realized by the Gauss map of some conformal immersion  $f : M \rightarrow \text{Im } \mathbb{H}$  (see [Kamberov et al. 2002, pg 8]).

Moreover, notice that any complex structure  $J$  induces a direct sum decomposition of the space  $\text{Hom}(TM, \mathbb{R}^3)$  of  $\mathbb{R}^3$ -valued functions on  $TM$  analogous to that from classical complex analysis. In particular, given  $\alpha \in \text{Hom}(TM, \mathbb{R}^3)$  there are conformal resp. anti-conformal parts of  $\alpha$  with respect to  $f$ ,

$$\alpha^+ = \frac{1}{2} (\alpha - N * \alpha), \quad \alpha^- = \frac{1}{2} (\alpha + N * \alpha),$$

and it is easily checked that  $*\alpha^+ = N \alpha^+$  while  $*\alpha^- = -N \alpha^-$ . This leads to a natural definition of quasiconformality in the quaternionic setting.

**Definition 3.2.** Let  $M \subset \mathbb{R}^3$  be an immersed surface with complex structure  $J : TM \rightarrow TM$  realized by its Gauss map  $N : M \rightarrow S^2$ . Then, a mapping  $f : M \rightarrow \text{Im } \mathbb{H}$  is said to be quasiconformal

provided there exists a measurable,  $\mathbb{C}$ -antilinear endomorphism  $\mu : TM \rightarrow TM$  which satisfies  $|\mu|_\infty < 1$  and

$$df^- = df^+ \circ \mu.$$

Definition 3.2 is the quaternionic analogue of the standard definition for abstract Riemann surfaces  $(M, J)$  given in Section 2. On the other hand, the algebraic structure of  $\mathbb{H}$  enables an equivalent criterion which is more useful for practical computation and makes explicit use of quaternionic multiplication. First, note that the BC  $\mu$  can be interpreted as a function  $\tilde{\mu} : TM \rightarrow (TM)^\perp$  taking values in the normal bundle to  $TM$  in  $\mathbb{H}$ , which is isomorphic to the complex plane at every point (simply choose  $N$  as the imaginary unit). To see this, consider a local domain  $U \subset M$  with section  $v \in TU$  and write  $\mu : TU \rightarrow TU$  as

$$\mu(v) = \mu^1(v)v + \mu^2(v)Jv,$$

for some “coordinate” functions  $\mu^i : TU \rightarrow \mathbb{R}$ . Consequently, it follows that

$$\begin{aligned} df^+ \circ \mu(v) &= df^+ \left( \mu^1(v)v + \mu^2(v)Jv \right) \\ &= \mu^1(v)df^+(v) + \mu^2(v)*df^+(v) \\ &= (\mu^1(v) + \mu^2(v)N)df^+(v) = \tilde{\mu}(v)df^+(v), \end{aligned}$$

where  $\tilde{\mu} = \mu^1 + \mu^2 N$  is a  $(TU)^\perp$ -valued function on  $TU$ . The reversibility of this argument establishes that normal-valued quaternionic functions  $\tilde{\mu}$  satisfying  $|\tilde{\mu}|_\infty < 1$  (which transform appropriately as defined by Lemma 3.4) correspond precisely to the BCs of quasiconformal mappings  $f : M \rightarrow \mathbb{R}^3$ , giving an alternative representation of these objects. This leads to the following equivalent to Definition 3.2 which is illustrated in Figure 8.

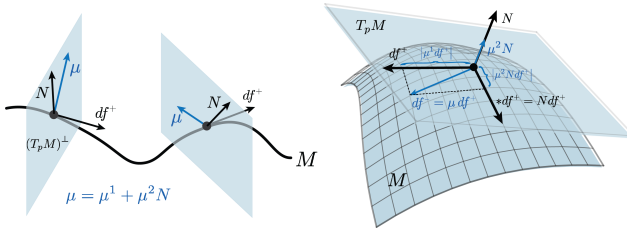


Fig. 8. Left: an illustration of  $\mu$  as a normal-valued quaternion field. Right: an illustration of Definition 3.3.

**Definition 3.3.** Let  $M \subset \mathbb{R}^3$  be an immersed surface with complex structure  $J : TM \rightarrow TM$  defined by its Gauss map  $N : M \rightarrow \mathbb{S}^2$ . Then, a mapping  $f : M \rightarrow \text{Im } \mathbb{H}$  is said to be quasiconformal provided there exists a measurable, normal-valued quaternion field  $\mu : TM \rightarrow (TM)^\perp$  which satisfies  $|\mu|_\infty < 1$  and

$$df^- = \mu df^+.$$

The equality in Definition 3.3 is suggestive of the coordinate-dependent expression  $f_z = \mu f_z$  seen in the planar case, but has the notable benefit of being expressed without reference to any underlying coordinate system. From this definition, it is straightforward to establish how  $\mu : TM \rightarrow (TM)^\perp$  must transform under a change of basis for  $TM$ .

**LEMMA 3.4.** Let  $a \in \mathbb{C}$ ,  $a = a^1 + Ja^2$  and suppose  $\mu : TM \rightarrow (TM)^\perp$  is a Beltrami coefficient satisfying Definition 3.3. Then, for any local domain  $U \subset M$  with section  $v \in TU$  it follows that

$$\mu(av) = \frac{\bar{a}^2}{|a|^2} \mu(v),$$

where  $a \in \mathbb{H}$ ,  $a = a^1 + Na^2$  is the quaternionic analogue of  $a$ .

**PROOF.** Due to the conformality (resp. anticonformity) of  $df^+$  (resp.  $df^-$ ), it follows that

$$\begin{aligned} a\mu(av)df^+(v) &= (\mu df^+)(av) = df^-(av) \\ &= \bar{a}df^-(v) = \bar{a}(\mu df^+)(v) = \bar{a}\mu(v)df^+(v). \end{aligned}$$

Therefore,  $\mu(v) = (\bar{a}/a)\mu(av)$  and the conclusion follows.  $\square$

In the literature on quasiconformal maps, a bounded measurable function  $\mu$  that transforms in this way is said to be a “(-1,1)-form” on  $TM$  (c.f. [Hubbard 2006, Section 4.8]). In particular, given a local conformal coordinate  $z$  on a domain  $U \subset M$ , several authors write the suggestive expression  $\mu = \hat{\mu} \frac{d\bar{z}}{dz}$  for some local function  $\hat{\mu} : U \rightarrow \mathbb{C}$  to illustrate the transformation rule seen in Lemma 3.4. More tensorially, any  $\mathbb{C}$ -antilinear  $\mu : TM \rightarrow TM$  as in Definition 3.2 can be expressed locally as  $\mu = \hat{\mu} d\bar{z} \otimes \frac{\partial}{\partial z}$ , so that for any  $a \in \mathbb{C}$ ,

$$\mu(av) = \hat{\mu} d\bar{z}(av) \frac{\partial}{\partial z} = \bar{a}\hat{\mu} d\bar{z}(v) \frac{\partial}{\partial z} = \bar{a}\mu(v).$$

It is remarkable that the same transformation rule is readily established in the quaternionic setting without reference to any particular system of local coordinates.

### 3.2 Beltrami versus Hopf

Definition 3.3 provides a link between the intrinsic quasiconformal geometry of  $M$  and its extrinsic immersion in  $\mathbb{R}^3$  which is useful for computing quasiconformal mappings between immersed surfaces. Before considering a minimization-based approach to accomplishing this in the present setting and its consequences for QC Iteration, it is worth discussing the BC  $\mu : TM \rightarrow (TM)^\perp$  in greater detail to gain some intuition about this new notion. In particular, let  $(M, J)$  be a Riemann surface with complex structure  $J$  induced by some Gauss map  $N : M \rightarrow \mathbb{S}^2$  as before. Then, the differential of any immersion  $f : M \rightarrow \mathbb{R}^3$  splits as  $df = df^+ + df^-$  with respect to  $J$ , so that its induced metric on  $M$  is given by

$$f^*\delta = |df|^2 = |df^+|^2 + |df^-|^2 + 2\operatorname{Re}(df^+\overline{df^-}),$$

where it was used that  $\langle v, w \rangle_{\mathbb{H}} = (1/2)(v\bar{w} + w\bar{v}) = \operatorname{Re}(v\bar{w})$ . The  $(2,0)$ -part of this quantity is the classical *Hopf differential* of the mapping  $f$ ,

$$Q = df^+\overline{df^-},$$

which quantifies deviation from conformality with respect to  $J$ . Expanding the positive and negative parts of this expression yields the alternative representation

$$4Q = |df|^2 - |*df|^2 - 2\langle df, *df \rangle N,$$

which shows that the Hopf differential is normal-valued, i.e. locally expressible on  $U \subset M$  as  $Q(v) = a(v) + b(v)N$  for some smooth functions  $a, b : TU \rightarrow \mathbb{R}$ . Moreover, it is clear from this expression that  $f$  is conformal or anticonformal if and only if  $Q \equiv 0$ . Conversely,



Fig. 9. Another view of the Teichmüller extremal mapping from Figure 5 but with 95% height deformation at the boundary. Note the visible structure of the quadratic differential governing the mapping, in particular the simple pole in front and simple zero on back which counteract to maintain zero Poincaré-Hopf index.

when  $f$  is quasiconformal in the sense of Definition 3.3, simple algebraic manipulations show that  $Q = \bar{\mu} |df^+|^2$  or alternatively

$$\mu = * \bar{Q},$$

demonstrating that the Beltrami differential  $\mu : TM \rightarrow (TM)^\perp$  characterizing quasiconformality is simply the conjugate of the Hopf differential up to an application of the Hodge star. Indeed, the structure of this object is often visible in the mapping (see e.g. Figure 9), where poles and zeroes necessarily appear according to the form of  $Q$ .

**Remark 3.5.** The relationship between  $\mu$  and  $Q$  discussed here can also be considered a (rearranged) special case of the isomorphism  $\tau \mapsto df^+ \tau$  between tangential-valued anticonformal one-forms and normal-valued quadratic differentials induced by the conformal immersion  $df^+ : M \rightarrow \mathbb{R}^3$  (see [Kamberov et al. 2002][Section 1.8] for details).

#### 4 MINIMIZING THE QUASICONFORMAL DISTORTION

It is now possible to discuss the present method for computing quasiconformal mappings directly from immersed surfaces, which is based on the quaternionic Definition 3.3. While the notion of quasiconformality in Definition 3.3 could be extended to cover the case of mappings  $f : M \rightarrow P$  between fixed Riemann surfaces  $M, P \subset \mathbb{R}^3$ , the present discussion will focus on mappings  $f : M \rightarrow f(M) \subset \mathbb{R}^3$  whose target is determined by the mapping itself, as this is the case most relevant for the remeshing and boundary deformation applications considered in Section 6. Figure 10 gives a qualitative example of this, where quasiconformal mappings are used to regularly interpolate some given boundary data. In this setting, the Riemann surface  $(M, J) \in \mathbb{R}^3$  is assumed given with complex structure  $J$  realized by its Gauss map  $N : M \rightarrow \mathbb{S}_2$ . Then, the quasiconformal distortion of a map  $f : M \rightarrow \mathbb{R}^3$  has the expression,

$$QC_\mu(f) = \int_M |df^- - \mu df^+|^2 dS_g,$$

which by Theorem A.1 in Appendix A is related to the conformal part of the Dirichlet energy with respect to the metric  $g(\mu)$  on  $M$  inherited from the BC  $\mu$ . Since the metric  $g$  and normal  $N$  to  $M$  are fixed, the conformal/anticonformal parts  $d(\cdot)^-, d(\cdot)^+$  and the Hodge star  $*$  are linear operators. Therefore,  $QC_\mu$  is a convex function of  $f$  (for fixed  $\mu$ ) whose global minimizer in each homotopy class is a least-squares quasiconformal mapping approximately satisfying Definition 3.3. This means quasiconformal mappings can be computed from compatible BCs  $\mu : TM \rightarrow (TM)^\perp$  by solving the minimization problem

$$\operatorname{argmin}_{f \in [f_0]} QC_\mu(f), \quad f|_{\partial M} = f_0|_{\partial M},$$

where  $f_0 : M \rightarrow \mathbb{R}^3$  is a suitable “initial” mapping whose boundary is prescribed and which defines the homotopy class under consideration. Expressing the unknown mapping  $f$  perturbatively in terms of a one-parameter family  $f(x, t) = f(x) + t\varphi(x)$  for  $t \in (-\varepsilon, \varepsilon)$  and some compactly supported variation  $\varphi : M \rightarrow \mathbb{R}^3$  vanishing on the boundary  $\partial M$ , standard techniques from the calculus of variations yield a necessary and sufficient criterion for  $f$  to be a minimizer of  $QC_\mu$ . In particular, using the fact that  $\mu$ , the conformal structure, and the metric  $g$  are fixed, the derivative of the functional  $QC_\mu$  at  $f$  in the direction  $\varphi$  is given by

$$\begin{aligned} \delta QC_\mu(f)\varphi &:= \frac{d}{dt} \Big|_{t=0} QC_\mu(f + t\varphi) \\ &= \int_M \langle df^- - \mu df^+, d\varphi^- - \mu d\varphi^+ \rangle dS_g, \end{aligned}$$

where  $\langle \cdot, \cdot \rangle$  denotes the Euclidean inner product which takes place following the quaternionic products in its arguments. This can be written as a linear system of equations for the minimizer  $f$  once an appropriate basis of test functions is given, and specific details will be given in Section 4.3. On the other hand, notice that the above minimization does not constrain the surface area or extrinsic geometry of the image surface  $f(M)$  in  $\mathbb{R}^3$ , meaning that  $f(M)$  may be quite different qualitatively than  $M$ . While this is expected and not necessarily a problem, it is often desirable (e.g. when remeshing) to have constraints on the mapping  $f$  which keep the target surface close to the original in some sense. Therefore, the remainder of this Section discusses two constraints which are useful for this purpose, along with the specific finite element algorithm used at present for computing least-squares quasiconformal mappings.

##### 4.1 Preserving extrinsic geometry

As mentioned, it is often useful to compute quasiconformal mappings which preserve the extrinsic geometry of the source surface  $M \subset \mathbb{R}^3$ . Particularly when remeshing, a quasiconformal map  $f : (M, g_{\text{ref}}) \rightarrow (M, g)$  is desired which optimizes mesh element angles while preserving the original Gauss map  $N$  as well as possible (note that here the conformal structure  $[g_{\text{ref}}]$  is not inherited from the original immersion). Certainly, preserving  $N$  exactly is not possible unless  $f$  is a conformal mapping, although reasonably good agreement can be enforced in any case by using an appropriate constraint alongside the minimization of  $QC_\mu$ . One effective option for this was proposed in [Gruber and Aulisa 2020] for the purposes of preserving extrinsic features while minimizing the conformal

distortion, a functional which is equivalent to  $QC_\mu$  when  $\mu \equiv 0$  and arises in the context of least-squares conformal mapping. To describe this idea specifically, consider a point  $x \in M$ , an immersion  $f : M \rightarrow \mathbb{R}^3$ , and a curve  $\exp_x(tv)$  for some  $v \in T_x M$  and  $|t| < \varepsilon$ . The image of this curve lies on the immersed surface  $f(M)$ , and letting  $N$  be normal to the image  $f(M)$ , Taylor expansion around  $t = 0$  yields

$$f(\exp_x(tv)) = f(x) + t df(v) + \frac{t^2}{2} (\nabla df)(v, v) + O(t^3),$$

$$N\left(\exp_x\left(\frac{t}{2}v\right)\right) = N(x) + \frac{t}{2} dN(v) + O(t^2),$$

where  $df, \nabla df, dN$  are localized at  $x$ . Since  $\langle N, df(v) \rangle = 0$  pointwise for all  $v \in TM$ , it follows by differentiation that

$$\langle dN(v), df(v) \rangle + \langle N, (\nabla df)(v, v) \rangle = 0,$$

and therefore the difference vector  $f(\exp_x(tv)) - f(x)$  satisfies

$$\langle f(\exp_x(tv)) - f(x), N\left(\exp_x\left(\frac{t}{2}v\right)\right) \rangle = 0 + O(t^3).$$

This means that the inner product of the difference vector  $f(\exp_x(tv)) - f(x)$  with the normal vector in the middle vanishes to second order, inspiring a constraint for the shape-controlled minimization of  $QC_\mu$ . In particular, to keep the image of  $f$  close to the given reference immersion  $\mathbb{1}_M$  it is reasonable to require that

$$\langle f(x) - \mathbb{1}_M(x), N_{mid}(x) \rangle = 0,$$

where  $N_{mid} = (1/2)(N_{old} + N_{new})$  approximates the normal halfway between the image of  $\mathbb{1}_M$  and the image of  $f$ . This ensures that the difference vectors between the points of  $M$  and  $f(M)$  remain nearly tangential to the same implicit “surface” halfway between them, and can be implemented as a (nonlinear) constraint during the minimization of  $QC_\mu$  using a Lagrange multiplier.

For the purposes of this work, it is enough to choose  $N = N_{old}$ , giving a linearized version of this constraint which preserves the convexity of the problem. In particular, consider finding a pair of functions  $v : M \rightarrow \mathbb{R}^3$  and  $\rho : M \rightarrow \mathbb{R}$  which satisfy

$$\operatorname{argmin}_{v, \rho} \left( QC_\mu(\mathbb{1}_M + v) + \int_M \rho \langle v, N \rangle dS_g + \frac{\varepsilon}{2} \int_M \rho^2 dS_g \right),$$



Fig. 10. Two qualitatively different quasiconformal mappings (left, middle) from the torus with boundary (right) computed by minimizing  $QC_\mu$  with Algorithm 1 with different boundary conditions. See Figure 16 in Section 6 for a quantitative view.

where  $\varepsilon > 0$  is a fixed penalty parameter and  $v|_{\partial M} = 0$ . Then,  $f = \mathbb{1}_M + v$  minimizes  $QC_\mu$  and satisfies the desired constraint. Formulated weakly, desired pair  $v, \rho$  should satisfy the system

$$0 = \delta QC_\mu(\mathbb{1}_M + v) \varphi + \int_M \rho \langle \varphi, N \rangle dS_g,$$

$$0 = \int_M \psi \langle v, N \rangle dS_g + \varepsilon \int_M \psi \rho dS_g,$$

for all suitable variations  $\varphi : M \rightarrow \mathbb{R}^3$  and  $\psi : M \rightarrow \mathbb{R}$ . The mapping  $f = \mathbb{1}_M + v$  which minimizes this modified problem is then quasiconformal with normal field  $N$  suitably close to that of the original surface  $M$ . Figure 11 and others in Section 6 show that this procedure is suitable for producing quasiconformal maps which preserve extrinsic features even around corners and delicate contours in the mesh such as facial expressions.

**Remark 4.1.** Here, the penalty parameter  $\varepsilon \approx 10^{-5}$  is used to ensure  $L^2$ -regularity for the Lagrange multiplier  $\rho$ .

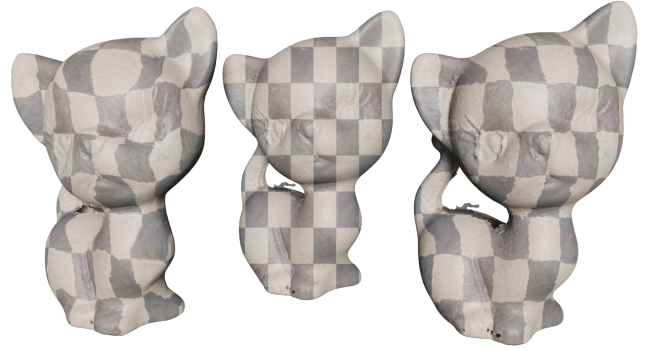


Fig. 11. Optimal quasiconformal remeshings of a cat with genus 1 and 19 boundary components with respect to an equi-angular conformal structure (c.f. Section 6.2). The original surface (middle) is mapped through QC Iteration with preserved extrinsic geometry (right) and preserved area (left). See Figure 19 in Section 6 for a quantitative view.

## 4.2 Preserving surface area

Recall that the minimizing the quasiconformal distortion  $QC_\mu$  in the metric  $g$  is equivalent to minimizing the Dirichlet energy  $\mathcal{D}_{g(\mu)}$  in the metric  $g(\mu)$  when the area of the target is fixed (see Appendix A for details). Since this area is variable when the target surface is defined implicitly through the mapping  $f$ , it is useful to have a constraint which fixes this quantity. This provides a reliable way to produce constrained harmonic maps which often improves the numerical results, especially in the case of the QC Iteration seen in Section 5. The present constraint follows by considering the surface area functional  $\mathcal{A}$ , defined as

$$\mathcal{A}(f) = \int_M 1 dS_{f^* \delta} = \int_M \frac{N}{2} df \wedge \overline{df}.$$

Standard techniques give the derivative of  $\mathcal{A}$  at  $f$  in the direction  $\varphi$ ,

$$\delta \mathcal{A}(f) \varphi = \int_M \langle df, d\varphi \rangle dS_{f^* \delta},$$

yielding a nonlinear constraint that can be implemented alongside the minimization of  $QC_\mu$ . On the other hand, the applications in Section 6 will almost always consider  $f = \mathbb{1}_M + v$  for some perturbation  $v : M \rightarrow \mathbb{R}^3$  as before. To retain convexity of the minimization in this case, it is reasonable to consider a heuristic constraint which is linear and exhibits good practical behavior. To that end, recall that the area element  $dS_{\mathbb{1}_M^* \delta} = |d\mathbb{1}_M|^2$  since  $\mathbb{1}_M$  is conformal (c.f. Appendix A), so that the area of  $M$  in terms of its reference metric  $g = \mathbb{1}_M^* \delta$  can be expressed as

$$A_0 := \mathcal{A}(\mathbb{1}_M) = \int_M |d\mathbb{1}_M|^2.$$

It follows that the difference in area between  $f(M)$  and  $M$  can be approximated by quantities depending only on  $g$ ,

$$\mathcal{A}(f) - A_0 = \int_M 1 dS_f^* \delta - \int_M |d\mathbb{1}_M|^2 \approx \int_M \langle d\mathbb{1}_M, dv \rangle dS_g.$$

With this, consider computing functions  $f : M \rightarrow \mathbb{R}^3$  and  $\lambda : M \rightarrow \mathbb{R}$  which satisfy

$$\operatorname{argmin}_{v, \lambda} \left( QC_\mu(\mathbb{1}_M + v) + \lambda \int_M \langle d\mathbb{1}_M, dv \rangle dS_g \right),$$

where  $v|_{\partial M} = 0$  and  $A_0 = \mathcal{A}(\mathbb{1}_M)$ . This is a convex minimization problem (over an appropriate function space) whose global solution can again be computed from weak-form equations. In particular, the desired pair  $v, \lambda$  should satisfy the system

$$\begin{aligned} 0 &= \delta QC_\mu(\mathbb{1}_M + v) \varphi + \lambda \int_M \langle d\mathbb{1}_M, d\varphi \rangle dS_g, \\ 0 &= \psi \int_M \langle d\mathbb{1}_M, dv \rangle dS_g, \end{aligned}$$

for all suitable variations  $\varphi : M \rightarrow \mathbb{R}^3$  and  $\psi : M \rightarrow \mathbb{R}$ . The unique mapping  $f$  satisfying this system is both a minimizer of  $QC_\mu$  and an approximately constrained harmonic mapping in the metric  $g(\mu)$ .

**Remark 4.2.** Note that the above system is underdetermined when the surface is closed, since only derivatives of the test functions are used. Therefore, the position of one point on  $M$  is fixed whenever this is the case.

#### 4.3 Minimization Algorithm

The final goal of this Section is to describe in detail the present algorithm for computing minimizers of  $QC_\mu$  in the framework of piecewise linear finite elements. Here it is assumed that the source surface  $M_h \approx M$  is given as a structured or unstructured orientable manifold mesh of triangles or quadrilaterals which are not degenerate. This implies that the interior angles of each element must be bounded below, although this bound may be very close to zero in practice as in the case of Figures 1 and 19. Under this assumption,  $M_h$  can be expressed as the union

$$M_h = \bigcup_{T \in \mathcal{I}} T,$$

where each  $T$  is a polygonal element of the discrete surface indexed by  $\mathcal{I}$ . Additionally, it will be assumed that the vertices of  $M_h$  are embedded in  $\mathbb{R}^3$ , so that  $M_h \subset \mathbb{R}^3$  carries a submanifold structure via the usual inclusion mapping  $\mathbb{1}_{M_h} : M_h \rightarrow \mathbb{R}^3$ . In practice,

it is convenient to “coordinatize”  $M_h$  with local parametrizations  $X_h : U_h \rightarrow M_h$  so that  $\mathbb{1}_{M_h} \circ X_h = X_h$  and each element  $T$  is the image of a reference (or parent) polygon  $\hat{T} \subset \mathbb{R}^2$  (warning: this is reversed from the usual notion of coordinate chart). This implies that functions on  $M_h$  may be discretized using a piecewise-linear polynomial basis (or tensor product of these) supported on each reference element (see e.g. [Dziuk and Elliott 2013, Section 4.3-4.4]). In particular, if the preimages through  $X_h$  of the  $n$  nodes of  $M_h$  are denoted by  $\{v_\alpha\}_{\alpha=1}^n$ , the standard Lagrange nodal basis  $\{\phi_\alpha\}_{\alpha=1}^n$  on  $U_h$  satisfies  $\phi_\alpha(v_\beta) = \delta_{\alpha\beta}$  for all  $1 \leq \alpha, \beta \leq n$ . The space of piecewise-linear finite elements on  $U_h$  can then be expressed as

$$\operatorname{Span}\{\phi_\alpha\} = \{\phi \in C^0(U_h) : \phi|_{\hat{T}} \in \mathbb{F}_1(\hat{T}), T \in \mathcal{T}\},$$

where  $\mathbb{F}_1$  denotes the space of linear polynomials  $\mathbb{P}_1$  when  $T$  is triangular and the tensor product space  $\mathbb{Q}_1$  when  $T$  is quadrangular. Note that this defines an analogous (nonlinear) basis  $\varphi = \phi \circ X_h$  for functions on the surface  $M_h$ .

**Remark 4.3.** To simplify the presentation, the remainder of the manuscript assumes the Einstein summation convention. Therefore, any tensor index appearing twice in an expression (once up and once down) is implicitly summed over its appropriate range. Similarly, the subscript  $h$  on discrete quantities will be omitted when the context is clear.

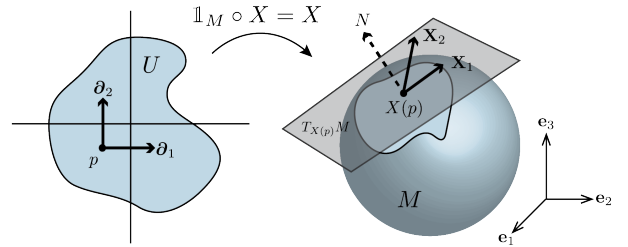


Fig. 12. The parametrization  $X$  coordinatizes a portion of the surface  $M$ . The vector fields  $\partial_i$  form a basis for  $T_p U$ , while their images  $X_i = dX(\partial_i)$  form a basis for  $T_{X(p)} M$ .

To describe the present discretization more precisely, suppose the smooth surface  $M$  is coordinatized by local parameterizations, each of which looks like  $X : U \rightarrow M$  for some domain  $U \subset \mathbb{R}^2$  (see Figure 12). It follows that if  $\{x^1, x^2\}$  are coordinates on  $U$ , then  $\{\partial_1, \partial_2\}$  form the standard basis for  $T_U$  where  $\partial_i := \partial/\partial x^i$ . As usual, the domain  $U$  is endowed with the pullback metric  $g = X^* \delta$  so that  $X = \mathbb{1}_M \circ X$  is an isometry of  $M$  (and hence a conformal mapping  $U \mapsto M$ ). Therefore, the differential of  $X$  has the expression  $dX = X_i \otimes dx^i$  where  $dx^i(\partial_j) = \delta_j^i$  and  $X_i = dX(\partial_i)$  has an expression in terms of the standard basis  $\{\mathbf{e}_I\}_{I=1}^3$  for  $\mathbb{R}^3$ ,

$$X_i = X_I^J \mathbf{e}_J, \quad X_I^J = \frac{\partial X^J}{\partial x^i}.$$

This yields local expressions on  $U$  of the Riemannian metric  $g$  and area element  $dS_g$  of  $M \subset \mathbb{R}^3$  as well as the (outward-directed) unit

normal field to  $M$ , given componentwise as

$$\begin{aligned} g_{ij} &= \langle \mathbf{X}_i, \mathbf{X}_j \rangle, \\ dS_g &= \sqrt{\det g} dx^1 \wedge dx^2, \\ N &= \frac{\mathbf{X}_1 \times \mathbf{X}_2}{|\mathbf{X}_1 \times \mathbf{X}_2|}. \end{aligned}$$

Letting  $\{\omega^i\}$  be the dual basis to  $\{\mathbf{X}_i\}$  and  $g^{ij}$  be the components of the metric inverse defined by  $g^{ik}g_{kj} = \delta_j^i$ , the differential of any function  $f : M \rightarrow \mathbb{R}^3$  can be locally expressed on  $TM|_{X(U)} \subset T\mathbb{R}^3$  as

$$df = \mathbf{F}_i \otimes \omega^i = g^{ij} \mathbf{F}_i \otimes \mathbf{X}_j.$$

Pulled back to  $TU$  through  $F := f \circ X$ , the vector fields  $\mathbf{F}_i = df(\mathbf{X}_i) = dF(\partial_i)$  then have an expression in terms of the same standard basis  $\{\mathbf{e}_J\}$ ,

$$\mathbf{F}_i = F_i^J \mathbf{e}_J, \quad F_i^J = \frac{\partial(f \circ X)^J}{\partial x^i}.$$

These expressions enable a local description of the quasiconformal distortion  $QC_\mu$  on each parameterization domain  $U$ . First, note that the discrete BC  $\mu : TM_h \rightarrow (TM_h)^\perp$  can be conveniently stored as a single complex-valued function  $\mu(\mathbf{X}_1)$ , since Lemma 3.4 allows for the computation of any other  $\mu(\mathbf{v})$  from this value by expressing  $\mathbf{v} = a\mathbf{X}_1 + bJ\mathbf{X}_2$  for some  $a, b \in \mathbb{R}$ . In particular, it is convenient to define  $\mu_F := \mu(\mathbf{X}_1) = \mu \circ dX(\partial_1)$  giving a representation of  $\mu$  on each reference element. Since  $X$  is conformal, it follows that  $\mu(\mathbf{X}_2) = -\mu(\mathbf{X}_1) = -\mu_F$  (easily checked with Lemma 3.4), and the difference  $df^- - \mu df^+$  applied to the basis vector fields  $\{\mathbf{X}_i\}$  has the expression

$$\begin{aligned} (D_1 f^I) \mathbf{e}_I &:= dF^-(\partial_1) - \mu \circ dX(\partial_1) dF^+(\partial_1) \\ &= \left( (1 - \mu_F) F_1^I + (1 + \mu_F) N F_2^I \right) \mathbf{e}_I, \\ (D_2 f^I) \mathbf{e}_I &:= dF^-(\partial_2) - \mu \circ dX(\partial_2) dF^+(\partial_2) \\ &= \left( (1 + \mu_F) F_2^I - (1 - \mu_F) N F_1^I \right) \mathbf{e}_I, \end{aligned}$$

where the quantities  $\mu_F, N, \mathbf{e}_I$  are all quaternionic functions. Using  $\langle \mathbf{v}, \mathbf{w} \rangle = \operatorname{Re}(\mathbf{v}\bar{\mathbf{w}})$  along with  $\bar{\mathbf{v}}\mathbf{w} = \bar{\mathbf{w}}\mathbf{v}$  and the fact that the  $\mathbf{e}_I$  are pure imaginary yields a local expression for the integrand of  $QC_\mu$ ,

$$\begin{aligned} |df^- - \mu df^+|^2 &= g^{ij} \left\langle (D_i f^K) \mathbf{e}_K, (D_j f^L) \mathbf{e}_L \right\rangle \\ &= -g^{ij} \operatorname{Re} \left( D_i f^K \mathbf{e}_{K \times L} \overline{D_j f^L} \right), \end{aligned}$$

where it was convenient to introduce the notation

$$\mathbf{e}_{K \times L} = \begin{cases} \mathbf{e}_K \times \mathbf{e}_L & K \neq L, \\ -1 & K = L. \end{cases}$$

Putting this together, the quasiconformal distortion of the local image  $F(U)$  for any  $U \mapsto M$  has the representation

$$\begin{aligned} QC_\mu(f) &= \int_{X(U)} |df^- - \mu df^+|^2 dS_g \\ &= \int_U -g^{ij} \operatorname{Re} \left( D_i f^K \mathbf{e}_{K \times L} \overline{D_j f^L} \right) \sqrt{\det g} dx^1 \wedge dx^2, \end{aligned}$$

which can be computed elementwise and summed to give the distortion of the mapping  $f$  on the entirety of  $M$ .

---

**Algorithm 1** Least-squares quasiconformal solve for  $f$  given  $\mu$ .

---

**Require:** Surface  $M \subset \mathbb{R}^3$ , mapping  $\hat{f} : M \rightarrow \mathbb{R}^3$ . Beltrami coefficient  $\mu$ .

- 1: Let  $f = \hat{f} + f_\alpha \varphi^\alpha$ , so that  $F = \hat{F} + F_\alpha \phi^\alpha$ .
- 2: Compute the Jacobian of  $QC_\mu$ ,

$$\tilde{\mathcal{J}}_K^{\alpha\beta} = -2 \int_M g^{ij} \operatorname{Re} \left( D_i \varphi^\alpha \mathbf{e}_{K \times L} \overline{D_j \phi^{L\beta}} \right),$$

where  $\int_M$  is shorthand for  $\int_U \sqrt{\det g} dx^1 \wedge dx^2$ .

- 3: **if** Normal constraint is active **then**
- 4:   Initialize  $\rho = \hat{\rho} + \rho_\alpha \psi^\alpha$ .
- 5:   Compute the block  $2 \times 2$  Jacobian of the constraint

$$\mathcal{J} = \begin{pmatrix} \mathcal{J}_{11} & \mathcal{J}_{12} \\ \mathcal{J}_{21} & \mathcal{J}_{22} \end{pmatrix} = \begin{pmatrix} \tilde{\mathcal{J}} & \int_M \psi^\alpha \langle \phi^\beta, N \rangle \\ \int_M \psi^\beta \phi^\alpha N & \varepsilon \int_M \psi^\alpha \psi^\beta \end{pmatrix},$$

- 6:   Form the residual vector

$$\mathcal{R}^\beta = \mathcal{J}^{\alpha\beta} \cdot \hat{S}_\alpha, \quad \hat{S}_\alpha = (\hat{\mathbf{F}}_\alpha \quad \hat{\rho}_\alpha)^\top.$$

- 7:   Solve the linear system

$$\mathcal{J} \cdot S = -\mathcal{R}, \quad S_\alpha = (\mathbf{F}_\alpha \quad \rho_\alpha)^\top.$$

- 8: **else if** Area constraint is active **then**
- 9:   Initialize  $\lambda = \hat{\lambda}$ .
- 10:   Compute the block  $2 \times 2$  Jacobian of the constraint

$$\mathcal{J} = \begin{pmatrix} \mathcal{J}_{11} & \mathcal{J}_{12} \\ \mathcal{J}_{21} & \mathcal{J}_{22} \end{pmatrix} = \begin{pmatrix} \hat{\lambda} \int_M g^{ij} \phi_i^\alpha \phi_j^\beta & \int_M g^{ij} \langle \hat{\mathbf{F}}_i, \phi_j^\beta \rangle \\ \int_M g^{ij} \phi_i^\alpha \hat{\mathbf{F}}_i & 0 \end{pmatrix}.$$

- 11:   Augment  $\mathcal{J}_{11} += \tilde{\mathcal{J}}$ .
- 12:   Form the residual vector

$$\mathcal{R}^\beta = \mathcal{J}^{\alpha\beta} \cdot \hat{S}_\alpha, \quad \hat{S}_\alpha = (\hat{\mathbf{F}}_\alpha \quad \hat{\lambda})^\top.$$

- 13:   Solve the linear system

$$\mathcal{J} \cdot S = -\mathcal{R}, \quad S_\alpha = (\mathbf{F}_\alpha \quad \lambda)^\top.$$

- 14: **else**
- 15:   Form the residual vector  $\mathcal{R}^\beta = \hat{\mathcal{J}}^{\alpha\beta} \cdot \hat{S}_\alpha$  where  $\hat{S}_\alpha = \hat{\mathbf{F}}_\alpha$ .
- 16:   Solve the linear system  $\mathcal{J} \cdot S = -\mathcal{R}$  for  $S_\alpha = \mathbf{F}_\alpha$ .
- 17: **end if**
- 18: **return**  $F = f \circ X$ .

---

Generating linear systems for the minimization problems discussed in this Section is now straightforward. Recall that a discrete function  $f : M_h \rightarrow \mathbb{R}^3$  can be represented component-wise in the nodal basis  $\{\phi^\alpha\}$  for  $U_h$  as

$$F^K = (f \circ X)^K = F_\alpha^K \phi_i^\alpha,$$

where  $F_\alpha^K$  denotes the value of the  $K^{th}$  component of  $F$  at (global) node  $\alpha$ . It follows that the derivative of  $f$  in the direction  $\mathbf{X}_i$  is then

$$df(\mathbf{X}_i) = F_i^K \mathbf{e}_K = F_\alpha^K \phi_i^\alpha \mathbf{e}_K = \mathbf{F}_\alpha \phi_i^\alpha,$$

so that the variation of  $QC_\mu(f)$  can be expressed as the linear system ( $U = \cup U_h$ )

$$\begin{aligned} \mathcal{J}_K^{\alpha\beta} F_\alpha^K &:= \delta QC_\mu(f) \varphi^\beta \\ &= F_\alpha^K \int_U -2g^{ij} \operatorname{Re} \left( D_i \varphi^\alpha \mathbf{e}_{K \times L} \overline{D_j \varphi^\beta} \right) \sqrt{\det g} dx^1 \wedge dx^2, \end{aligned}$$

where  $\mathcal{J}$  is the Jacobian operator and the vector test function  $\varphi^\beta = \varphi^{L\beta} \mathbf{e}_L$  is simply three independent copies of the nodal vector  $\varphi^\beta$ , since the test functions for each coordinate are the same. Expressing  $f = \hat{f} + f_\alpha \varphi^\alpha$  for some known function  $\hat{f} : M \rightarrow \mathbb{R}^3$  (such as  $\hat{f} = \mathbb{1}_M$ ) then yields the linear system

$$\mathcal{J} \cdot S = -\mathcal{R}, \quad \mathcal{R}^\beta = \mathcal{J}^{\alpha\beta} \cdot \hat{F}_\alpha = \mathcal{J}_K^{\alpha\beta} \hat{F}_\alpha^K,$$

which is readily solved for the nodal values  $\hat{F}_\alpha^K$ . The desired mapping  $F = f \circ X$  is then reconstructed from these values by linear interpolation over the mesh. Note that the constraints from Sections 4.1 and 4.2 can be discretized analogously and included along with this procedure, leading to the least-squares quasiconformal mapping procedure described in Algorithm 1. The examples from this paper were implemented in the open source finite element library FEMuS [Aulisa et al. 2014], and the Boost library [Schäling 2011] was used to compute the relevant quaternion products.

**Remark 4.4.** Since Algorithm 1 is formulated for mappings with an implicit target, it is not immediately obvious if it also has advantages in the more traditional setting of mappings between fixed Riemann surfaces  $M \mapsto P$  both given as e.g. manifold meshes in  $\mathbb{R}^3$ . On the other hand, since the geometry of  $P$  is known, constraints like those introduced here can certainly be implemented to keep the image of  $M$  close to  $P$  in an appropriate sense. This is essentially what is done in the remeshing examples to keep the image from “spilling out” of the original surface.

## 5 QUATERNIONIC QC ITERATION

Algorithm 1 provides a novel technical tool for computing quasiconformal mappings between immersed surfaces in Euclidean space, and can be applied when the target surface is explicit or implicit (c.f. Remark 4.4). As an interesting application of this new technology, consider how Algorithm 1 can be used to facilitate the QC Iteration from Section 2.3 in this more general setting. First, note that all the theory regarding extremal quasiconformal mappings discussed in Section 2.1 translates immediately to the quaternionic setting of maps  $f : M \rightarrow f(M) \subset \mathbb{R}^3$ . In particular, extremal Teichmüller mappings or close approximations thereof exist in every homotopy class of maps relative to  $\partial M$ , and these mappings have uniform conformality distortion across their domain.

As previously mentioned, the QC iteration algorithm from [Lui et al. 2015, 2014] is an approach to computing Teichmüller mappings through the relationship of the quasiconformal distortion  $QC_\mu$  to the Dirichlet energy  $\mathcal{D}_{g(\mu)}$ . More precisely, the goal is to use minimizers of  $QC_\mu$  (for fixed  $\mu$  and fixed homotopy class  $[f_0]$ ) to construct a sequence of BCs  $\{\mu_k\}_{k=0}^{n_t}$  (number of iterations  $n_t > 0$ ) which converges to a function  $\mu_{n_t}$  that is approximately Teichmüller, i.e. that approximately satisfies Definition 2.1. Accomplishing this requires a way to compute quasiconformal mappings  $f$

given  $\mu$ , along with a procedure which encourages  $\mu$  to have the correct local structure at each iteration  $1 \leq k \leq n_t$ . It will now be shown that the quaternionic technology from Section 3 and the least-squares quasiconformal mapping Algorithm 1 from Section 4 enable the modified QC Iteration outlined in Algorithm 2, which directly computes an approximately Teichmüller quasiconformal mapping  $f : M \rightarrow f(M) \subset \mathbb{R}^3$  satisfying prescribed Dirichlet boundary data. The remainder of this Section discusses each step of this algorithm in detail.

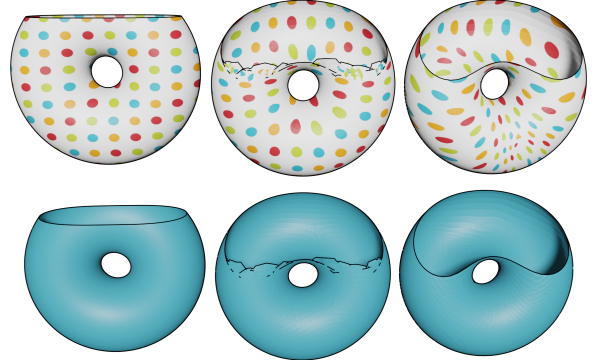


Fig. 13. Comparison of LSCM (mid) and Algorithm 2 (right) from a torus with boundary (left) to a similar surface with different boundary data. Here again the LSCM does not remain injective despite its much lower average distortion. Conversely, QC Iteration produces a natural looking map with near-uniform texture distortion (99% of elements with  $|\mu| \in [0.4, 0.5]$ ).

**Remark 5.1.** It is important to mention that the quaternionic QC Iteration Algorithm 2 cannot approximate Teichmüller mappings to arbitrary accuracy when  $M$  is not simply connected. This is a consequence of the local phase-based smoothing referred to in Remark 2.5 and discussed in Section 5.3. In this case, the QC Iteration will optimize for a BC with approximately constant norm which may or may not be close to an actual Teichmüller mapping. Regardless, practical results illustrate that high-quality quasiconformal mappings between multiply connected surfaces are achieved with Algorithm 2 despite this concern, e.g. Figures 13, 10, 9 and others in Section 6.

---

### Algorithm 2 Overview of the quaternionic QC Iteration

---

**Require:** Surface  $M \subset \mathbb{R}^3$  and homotopy class  $[f']$ . Beltrami coefficient  $\mu_0 = 0$ . Stopping tolerance  $\varepsilon > 0$  and maximum iteration number  $n_t > 0$ .

- 1: **while**  $0 \leq k \leq n_t$  and  $QC_{\mu_k}(f_k) > \varepsilon$  **do**
- 2:     (1) Given  $\mu_k$ , Minimize  $QC_{\mu_k}$  for  $f_k : M \rightarrow \mathbb{R}^3$ .
- 3:     (2) Compute  $\mu_{k+1}$  algebraically given  $f_k$ .
- 4:     (3) Post-process  $\mu_{k+1}$  to bring it closer to Teichmüller form.
- 5:     (4) Minimize  $QC_\mu(f_k)$  for  $\mu$  on the line between  $\mu_k$  and  $\mu_{k+1}$ , generating  $\mu_{k+1} \leftarrow \mu$ .
- 6: **end while**
- 7: **return**  $(f, \mu)$

---

### 5.1 Step 1: Computing Quasiconformal Mappings

Given a BC  $\mu : TM \rightarrow (TM)^\perp$ , the first task is to compute a corresponding map  $f : M \rightarrow \mathbb{R}^3$  which minimizes the quasiconformal distortion  $QC_\mu$ . The present method for accomplishing this was discussed at length in Section 4 and culminated in Algorithm 1, which is a linear procedure for computing a least-squares quasiconformal mapping when  $\mu$  is stored as a value per-element aligned with the vector field  $\mathbf{X}_1 = dX(\partial_1)$ . It is worth mentioning that the mapping computed in this process will generally not be harmonic with respect to the metric  $g(\mu)$  on  $M$  unless the target surface is made explicit or an area constraint such as that discussed in Section 4.2 is enforced. While this has consequences for the theory developed in [Lui et al. 2015], it does not seem to hinder the performance of the QC Iteration much in practice, as high-quality quasiconformal mappings are produced despite this aspect.

### 5.2 Step 2: Computing the Beltrami Coefficient

Once a particular quasiconformal mapping  $f : M \rightarrow \mathbb{R}^3$  has been determined, it is necessary to compute its Beltrami coefficient  $\mu$  in the complex structure determined by the Gauss map  $N$ . This reveals another substantial benefit of the quaternionic approach from Section 3: since  $\mathbb{R}^3 \cong \text{Im } \mathbb{H}$ , computing the desired function  $\mu : TM \rightarrow (TM)^\perp$  as in Definition 3.3 becomes a simple algebraic exercise captured by the follow Lemma.

**LEMMA 5.2.** *Let  $f : M \rightarrow \text{Im } \mathbb{H}$  be a quasiconformal mapping with respect to the complex structure induced by  $N : M \rightarrow S^2$ . Then, the Beltrami coefficient  $\mu : TM \rightarrow (TM)^\perp$ ,  $\mu = \mu^1 + \mu^2 N$  can be expressed component-wise as*

$$\mu^1 = \text{Re} \left( \frac{df^- \overline{df^+}}{|df^+|^2} \right), \quad \mu^2 = \text{Re} \left( \frac{df^- \overline{N df^+}}{|df^+|^2} \right),$$

**PROOF.** Since  $df^- = \mu df^+$ , the definition of the complex structure on  $TM$  induced by  $N$  yields

$$\frac{df^- \overline{df^+}}{|df^+|^2} = \mu^1 + \mu^2 N.$$

The desired representation now follows from multiplication by  $N$  and the fact that  $\overline{vw} = \overline{w}\overline{v}$  for quaternions  $v, w \in \mathbb{H}$ .  $\square$

This result provides a quick and straightforward way to extract the BC  $\mu$  of the least-squares minimizer  $f$  from Step 1 and is given in pseudocode as Algorithm 3. On the other hand, recall that the components of  $\mu$  are not invariant under changes of basis for  $TM$ , which has consequences for the present implementation since  $\mu_F = \mu(\mathbf{X}_1)$  is stored as a complex function per-element. In particular, the local calculations in Step 3 will require averaging  $\mu_F$  between mesh elements, making it necessary to compare values of  $\mu$  which are discretized using different basis vectors  $\mathbf{X}_1$ . This requires careful consideration of the previously established Lemma 3.4, which is the analogue of coordinate-dependence for quaternionic BCs.

### 5.3 Step 3: Post-processing the Beltrami Coefficient

Once the BC  $\mu$  has been computed from the most recent mapping  $f$ , the final step in the original QC iteration is to perturb it in a way which encourages Teichmüller form. More precisely, a combination

---

**Algorithm 3** Computation of  $\mu_F = \mu(\mathbf{X}_1)$  from  $f : M \rightarrow \mathbb{R}^3$ .

---

**Require:** Quasiconformal mapping  $f : M \rightarrow \mathbb{R}^3$ . Local parameterizations  $X : U \rightarrow M$  such that  $F = f \circ X$ .

1: Compute  $\mathbf{v}^+ = df^+(\partial_1)$  and  $\mathbf{v}^- = df^-(\partial_1)$ .

2: Compute the BC

$$\mu_F = \frac{\mathbf{v}^+ \bar{\mathbf{v}}^+}{|\mathbf{v}^+|^2}.$$

3: **return**  $\mu_F^1 = \text{Re}(\mu_F)$  and  $\mu_F^2 = -\text{Re}(\mu_F N)$ .

---

of projection on the norm  $|\mu|$  along with local Laplace smoothing on the phase  $e^{i \arg \mu}$  is performed in order to produce a BC which is closer to locally optimal as defined by Lemma 2.4. To accomplish this in the present quaternionic setting, it remains to discuss the details of the smoothing operations described in Section 2.3. First, recall that the BC  $\mu$  corresponding to the  $f$  from Step 1 is stored as a per-element value  $\mu_F = \mu(\mathbf{X}_1)$  which is aligned with the image of the basis vector  $\partial_1$  coming from the bottom edge of each reference element. From this data, it is straightforward to extract the polar decomposition  $\mu_F = |\mu_F| (\mu_F / |\mu_F|)$ , giving the per-element norm and phase of the BC which can be manipulated separately in an advantageous way. In particular, since Teichmüller BCs  $\mu = k\bar{q}/|q|$  have constant norm  $0 < k < 1$  and harmonic argument away from the zeros and poles of the quadratic differential  $q$  by Lemma 2.4, it is desirable to perturb these quantities in a way which encourages this structure. This is straightforward in the case of the norm  $|\mu_F|$ , and the present method comes immediately from [Lui et al. 2014]. Particularly, if  $n_T := |T|$  denotes the number of mesh elements, the average of the norms  $|\mu_F|$  is computed across the mesh,

$$|\mu|_{\text{avg}} = \frac{1}{n_T} \sum_{F=1}^{n_T} |\mu_F|,$$

which then replaces the value of  $|\mu_F|$  on each individual element of the mesh (see Algorithm 4). Seen abstractly, this can be considered a projection operation onto the space of constant-norm BCs.

The local smoothing operation performed on the phase  $e^{i \arg \mu_F} = \mu_F / |\mu_F|$  is more delicate due to the basis-dependence of  $\mu$  and is illustrated in Figure 14. While the main idea is still single-step Jacobi iteration as in [Lui et al. 2014], here it is necessary to compare the BCs  $\mu_F$  which are discretized over local vectors  $\mathbf{X}_1$  which are globally distinct. To describe this more precisely, consider a reference element on the parametrization domain  $U_h$  with basis vector  $\partial_1$  aligned with its bottom edge. Then, an adjacent edge making an angle  $\theta$  with the bottom edge carries a natural direction vector given by  $e^{i\theta} \partial_1 = \cos \theta \partial_1 + i \sin \theta \partial_1$ . Now, unless the image of this adjacent edge lies on the boundary  $\partial M_h$ , there is some other element of  $M_h$  which shares it, and (as the mesh is generally unstructured) the preimage of the corresponding edge belonging to this element may not make an angle of  $\theta$  with respect to its own bottom edge vector  $\partial_1$ . Therefore, it is not sufficient to simply average both representations  $\mu_F = \mu(\mathbf{X}_1)$  directly, as there is no guarantee that the tangent spaces of neighboring elements on  $M_h$  are properly aligned. On the other hand, it follows from Lemma 3.4 that the BC discretized on any tangent vector is computable from  $\mu(\mathbf{X}_1)$ , i.e. if

$a = e^{i\theta}$  then  $\mu(aX_1) = \bar{a}^2 \mu(X_1)$  (recall that  $X$  is conformal). Therefore, a local Jacobi iteration as in [Lui et al. 2014] is still feasible provided the discrete representations of  $\mu$  are adjusted in this way beforehand. Moreover, it is clear that the reflection  $aX_1 \mapsto -aX_1$  induces no change in  $\mu$ , so that the values of  $\mu$  on shared edges will be component-wise comparable.

In view of this discussion, the present smoothing on the phase of  $\mu$  involves first localizing the phase  $\mu_F/|\mu_F| = e^{i \arg \mu_F}$  to the edges of each mesh element, averaging its values there, and finally re-projecting these averaged values back into the elements (c.f. Algorithm 4). More precisely, consider an element  $\hat{T}$  and the positive angle  $\theta_i = \angle(\partial_1, E_i)$  which each edge vector  $E_i$  of  $\hat{T}$  makes with edge vector  $\partial_1$ . Then, the projection matrix from  $\hat{T}$  to local edge  $i$  follows directly from Lemma 3.4 and is built as

$$P(\theta_i) = \begin{pmatrix} \cos^2 \theta_i - \sin^2 \theta_i & -2 \cos \theta_i \sin \theta_i \\ 2 \cos \theta_i \sin \theta_i & \cos^2 \theta_i - \sin^2 \theta_i \end{pmatrix},$$

so that  $\mu_{F,i} := P(\theta_i)\mu_F$  (interpreted as matrix multiplication) gives the appropriate value of  $\mu_F$  on the  $i^{th}$  edge of  $\hat{T}$ . Doing this over all elements  $1 \leq \hat{T} \leq n_T$  gives the local per-edge phases  $\mu_{F,i}/|\mu_F|$  (note that  $\det P(\theta_i) = 1$ ) that can be averaged according to how many elements share each edge. In particular, since reversing the orientation of an edge does not change the value of the phase, it suffices to add the contributions of each local edge  $\mu_{F,i}/|\mu_F|$  to the global edge phase  $e^{i \arg \mu_\alpha}$ ,  $1 \leq \alpha \leq n_E$  and then divide by the number of elements sharing edge  $\alpha$ —either 1 or 2, for boundary or internal edges, respectively. This action yields a smoothed phase in each edge, which can be averaged back from the edges to the elements  $\hat{T}$  with the matrices  $P(\theta_i)^\top$ . Finally, once the norm and the phase of  $\mu_F$  have been independently averaged, the new BC on the each reference element  $\hat{T}$  is reconstructed as

$$\mu_F \leftarrow |\mu|_{\text{avg}} \mathcal{S}(e^{i \arg \mu_F}),$$

where  $\mathcal{S}$  denotes the local smoothing operation just discussed. Pseudocode for the entire procedure outlined this Subsection is given in Algorithm 4.

**Remark 5.3.** Notice that only one step of Jacobi iteration is performed during the post-processing of  $\mu_F$ . Empirically, more smoothing than this generally produces a QC Iteration terminating in a “worse” BC with less uniform distortion and a higher maximum value. Theoretically, this is related to the fact that the perturbation  $\mu + \epsilon v$  is not guaranteed to produce an energy  $\mathcal{E}(\mu + \epsilon v)$  which is smaller than  $\mathcal{E}(\mu)$  when  $\operatorname{Re} \int_M Q(f)v dS_g(\mu) < 0$ . Here  $Q(f)$  is the Hopf differential and  $\mathcal{E}$  is the “Beltrami energy” (see [Lui et al. 2015, Lemma 4.1] and Appendix B).

#### 5.4 Step 4: Ensuring the Distortion is Non-increasing

The final step in the quaternionic QC Iteration presented here is to ensure that the distortion  $QC_\mu$  does not increase during the perturbative Step 3. Recall from Remark 2.5 that the local smoothing on the phase of  $\mu_F$  is really a surrogate for similar smoothing on the argument, and these procedures are inequivalent for multiply connected  $M$ . Therefore, it is not guaranteed that Step 3 actually makes progress in every case, and it is useful to include a line search which forces the iteration to converge when no more progress can

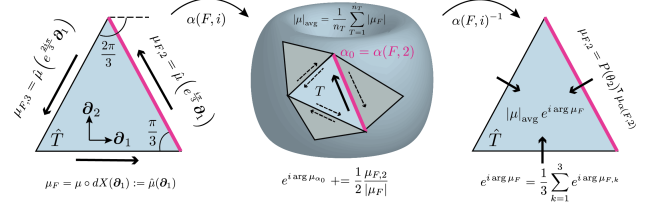


Fig. 14. Step 3 of the QC iteration in the discrete setting applied to an element with equilateral angles. Note the local averaging of the norm and phase as outlined in Algorithm 4.

---

#### Algorithm 4 Post-processing of $\mu_F$ .

```

Require: Triangulation (or quadrangulation)  $\mathcal{T}$  of the surface  $M$ 
with cardinality  $n_T$ , per-element values  $\mu_F$ , local-to-global edge
mapping  $\alpha(F, i)$ .
1: Initialize  $|\mu|_{\text{avg}} = 0$ 
2: for element  $1 \leq \hat{T} \leq n_T$  do
3:   Update  $|\mu|_{\text{avg}} += \frac{|\mu_F|}{n_T}$ 
4:   Normalize  $\mu_F \leftarrow \frac{\mu_F}{|\mu_F|}$ 
5: end for
6: for edge  $1 \leq \alpha \leq n_E$  do
7:   Initialize  $\mu_\alpha = 0$  and  $l_\alpha = 0$ 
8: end for
9: for element  $1 \leq \hat{T} \leq n_T$  do
10:   for edge  $1 \leq i \leq n_e$  do
11:     Compute  $\theta_i = \angle(\partial_1, E_i)$ 
12:     Update  $\mu_{\alpha(F,i)} += P(\theta_i) \mu_F$  and  $l_{\alpha(F,i)} += 1$ 
13:   end for
14: end for
15: for edge  $1 \leq \alpha \leq n_E$  do
16:   Average  $\mu_\alpha \leftarrow \frac{\mu_\alpha}{l_\alpha}$ 
17: end for
18: for element  $1 \leq \hat{T} \leq n_T$  do
19:   Initialize  $\mu_F = 0$ 
20:   for edge  $1 \leq i \leq n_e$  do
21:     Compute  $\theta_i = \angle(\partial_1, E_i)$ 
22:     Update  $\mu_F += \frac{1}{n_e} P(\theta_i)^\top \mu_{\alpha(F,i)}$ 
23:   end for
24:   Compute  $\arg \mu_F = \operatorname{atan2}(\mu_F^2, \mu_F^1)$ 
25: end for
26: return  $\mu_F \leftarrow |\mu|_{\text{avg}} e^{i \arg \mu_F}$ 

```

---

be made without increasing the value of  $QC_\mu$ . This is done by searching for the energetically optimal Beltrami coefficient on the straight line between the iterates  $\mu_k$  and  $\mu_{k+1}$  (c.f. Algorithm 5) when the previously computed mapping  $f_k$  is fixed. In particular, consider the linear combination

$$\mu(t) = t\mu_{k+1} + (1-t)\mu_k,$$

of the BC  $\mu_k$  from the beginning of iteration stage  $k$  and the smoothed BC  $\mu_{k+1}$  from Step 3. Then, using  $\dot{\mu} = \mu_{k+1} - \mu_k$  to denote differentiation with respect to the parameter  $t$ , the derivative of  $QC(f_k)$  is

given by

$$\frac{d}{dt} QC_\mu(f_k) = - \int_M \langle \dot{\mu} df_k^+, df_k^- - \mu df_k^+ \rangle dS_g,$$

where  $\langle \cdot, \cdot \rangle$  denotes the Euclidean inner product as before which happens after the quaternionic products in its arguments. Setting the above equal to zero and solving for  $t$  then yields the minimizing parameter value

$$t_0 = \frac{\int_M \langle \dot{\mu} df_k^+, df_k^- - \mu df_k^+ \rangle dS_g}{\int_M |\dot{\mu} df_k^+|^2 dS_g},$$

which corresponds to the optimal BC along this linear interpolation. Setting  $\mu_{k+1} \leftarrow \mu(t_0)$  then gives an updated BC which is used as input to the next iteration.

**Remark 5.4.** It is worth mentioning again that Step 4 is not present in the original QC Iteration of [Lui et al. 2014], and is not strictly necessary for it to be applied. On the other hand, faster convergence and better overall performance is observed when it is included, despite the fact that  $QC_\mu(f_k)$  is computed with respect to the previous iterate  $f_k$  and not the “current” least-squares quasiconformal minimizer  $f(t)$  corresponding to  $\mu(t)$ .

## 6 EXAMPLES AND APPLICATIONS

Now that the QC Iteration algorithm has been extended to the quaternionic setting of maps from immersed surfaces  $M \subset \mathbb{R}^3$ , some useful applications are discussed. While there are many varied uses for computational quasiconformal maps, the two discussed at present relate to object deformation and surface remeshing. Note that the histograms shown here and throughout the rest of the paper report the norm of the BC  $\mu$  with respect to a pre-specified conformal structure on  $M$  (computed by Algorithm 5 unless otherwise stated), and the vertical axis of each histogram displays the percentage of elements in each bin.

### 6.1 Object deformation

Certain tasks in animation and graphics require a natural looking map between objects which satisfies some prescribed boundary data. It will now be shown that Algorithm 1 and the quaternionic QC Iteration Algorithm 2 can be useful for this purpose by producing evenly distorted mappings which nicely interpolate some given boundary data. Qualitative examples of this have already been seen in Figures 9, 10, and 13, but it is enlightening to discuss more quantitative aspects of Algorithms 1 and 2 as well. Figure 15 shows how a genus zero surface with 6 boundary components is deformed by an optimal Teichmüller map computed with QC Iteration to satisfy the given boundary conditions. Here the structure of the mapping is nicely visible: the norm  $|\mu|$  is nearly constant and  $\mu$  is discontinuous at the zeroes and poles of its associated quadratic differential. Similarly, Figure 16 shows two optimal mappings satisfying different prescribed boundary data computed with Algorithm 2 from an open (genus 1) torus. Again, it can be seen that the BC  $\mu$  is discontinuous and relatively uniform across the target surfaces, as expected. Finally, Figure 17 and the previously seen Figure 5 provide quantitative views into the mappings seen in Figures 2 and Figure 9,

respectively. Notice from Figure 17 that the quaternionic QC Iteration is also applicable to planar domains by choosing any constant vector as normal, e.g.  $N = (0 \ 0 \ 1)^\top$ , and produces the expected results which respect injectivity by construction. Moreover, Figure 5 shows that injectivity can be preserved with Algorithm 5 even when the shape of the target surface is implicit using e.g. the constraint formulated in Section 4.1.

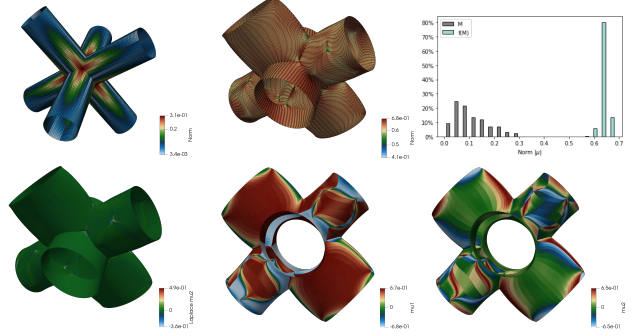


Fig. 15. An optimal quasiconformal mapping of a multiply connected domain computed using the (unconstrained) QC Iteration Algorithm 2 for prescribed boundary data. Top row: source and target surfaces (left, middle) colored by  $|\mu|$ , histogram of  $|\mu|$  (right). Bottom row: Laplacian  $\Delta\mu^1$  (left), components of the BC  $\mu$  (middle, right). Notice that  $\mu$  is discontinuous and nearly harmonic away from its zeros as expected.

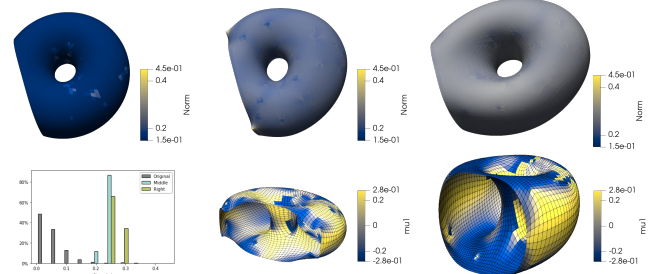


Fig. 16. A quantitative view of the tori from Figure 10 computed with the (unconstrained) QC Iteration Algorithm 2. Top row: source surface (left) and target surfaces (middle, right) computed for different given boundary data, colored by  $|\mu|$ . Bottom row: histogram (left),  $\mu^1$ -values (middle, right) for each surface above.

### 6.2 Surface remeshing

Most methods for solving PDEs on surface data are only as accurate as the mesh which discretizes the surface  $M$ . Here we show that the quaternionic QC Iteration can be useful for generating a more regular discretization of a given surface  $M \subset \mathbb{R}^3$  by optimizing the angles between mesh elements. To that end, suppose  $(M, g)$  is given where  $g = \mathbb{1}_M^* \delta$  is the metric inherited from the embedding of the vertex positions (note that this is only necessary to define the conformal class). The idea behind remeshing with Algorithm 1

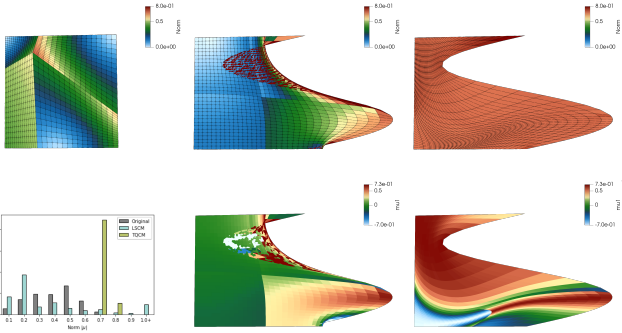


Fig. 17. A quantitative view of the LSCM and TQCM mappings in Figure 2 computed using a reference conformal structure of regular squares. Top row: source surface (left), LSCM (middle), and TQCM (right) all colored by  $|\mu|$ . Bottom row: histogram (left), plots of  $\mu^1$  (middle, right) for the mappings above.

is to find an optimal quasiconformal mapping  $f : (M, g_{\text{ref}}) \rightarrow (M, g)$  in the homotopy class of  $\mathbb{1}_M$  which preserves the extrinsic geometry of  $M$  but changes its conformal class in a beneficial way (quasiconformal to  $[g_{\text{ref}}]$ ), effectively making the mesh elements more regular. This can be done by carrying out the QC Iteration from Section 5 using the constraint formulated in Section 4.1, which will search for a dilatation-optimal map from the conformal class of a desired reference metric  $g_{\text{ref}}$  to the immersed surface which respects the surface normal  $N$ . Some examples of this are displayed in Figures 1, 20, 18, and 19, which show how the QC Iteration produces surfaces with near-uniform distortion despite the use of very irregular initial data.

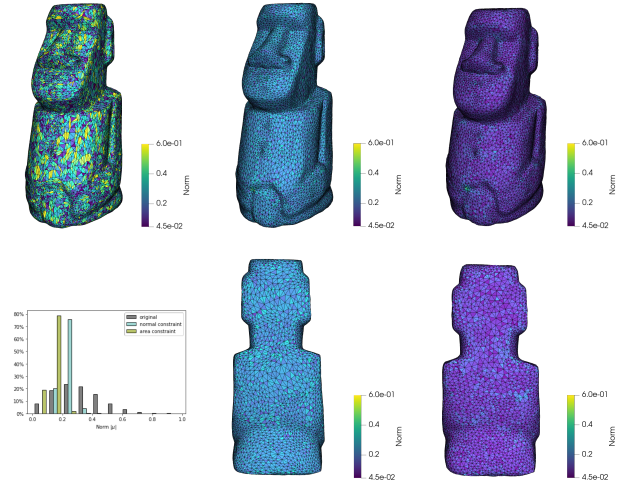


Fig. 18. QC remeshings of a moai statue (left) colored by  $|\mu|$ , constructed by QC Iteration with different constraints and with respect to the conformal structure given by Algorithm 5. Note that the normal constraint from Section 4.1 (middle) preserves extrinsic features with only minimal rounding of sharp features, while the area constraint from Section 4.2 (right) produces lower conformal distortion at the cost of a rounder extrinsic shape.

To elaborate on this procedure, note that the remeshing just described is dependent on the conformal class of the metric  $g_{\text{ref}}$ , i.e. on a set of interior angles provided by the user. This reflects the fact that  $QC_\mu$  will measure the (local)  $\mu$ -quasiconformal distortion of a mapping  $f \circ X : U \rightarrow \mathbb{R}^3$  with respect to a particular discretization  $U_h$  of  $U$ . In particular, the specific deviation from  $\mu$ -conformality will be reflected in the way mesh elements are distorted as they move from  $U_h$  into  $\mathbb{R}^3$  under this mapping, so it is important to pre-specify an appropriate configuration of angles on  $U_h$  to which the target surface  $f(M_h)$  should be quasiconformal. Of course, there is an obvious choice for this: simply pull back the initial triangulation/quadrangulation of  $M_h$  onto the reference domains  $U_h$  so that  $g_{\text{ref}} \in [g]$ . However, this is undesirable for at least two reasons. First, it is often the case that the angles coming from the initial configuration are nearly degenerate (see e.g. Figure 19 and Figure 1), so this choice is not useful if the goal is to improve the existing mesh on the surface. Second and most importantly, the identity mapping is always conformal (hence quasiconformal with distortion zero), so in fact this choice only produces a trivial minimizer which will not remesh the surface at all.

---

#### Algorithm 5 Generation of reference angles

---

**Require:** Reference discretization  $\mathcal{T}$  of the closed surface  $M$ .

```

1: for  $T \in \mathcal{T}$  do
2:   if  $T$  is triangle then
3:      $N_T = 3, \Theta = \pi$ 
4:   else if  $T$  is quadrilateral then
5:      $N_T = 4, \Theta = 2\pi$ 
6:   end if
7:   for vertex  $1 \leq i \leq N_T$  do
8:     Compute  $m_i = \#$  of adjacent elements
9:      $\alpha_i \leftarrow 2\pi/m_i$ 
10:  end for
11:  Determine maximum vertex angle  $\alpha_i$ .
12:  if  $\alpha_i > \alpha_j$  for all  $j \neq i$  then
13:     $\beta_i = \alpha_i$ 
14:    for vertices  $j \neq i$  do
15:       $\beta_j = \alpha_j (\Theta - \alpha_i) / (\sum_{k \neq i} \alpha_k)$ 
16:    end for
17:  else
18:    for vertices  $1 \leq j \leq N_T$  do
19:       $\beta_j = \alpha_j \Theta / (\sum_{k=1}^{N_T} \alpha_k)$ .
20:    end for
21:  end if
22: end for
23: return  $\beta$ 

```

---

Another simple and useful possibility for the reference discretization is to require the interior angles to be as close as possible to  $\pi/3$  in triangular elements and  $\pi/2$  for quadrangular elements. This encourages the target to be quasiconformally flat when the connectivity of  $M$  is perfectly regular, and provides a reasonable general purpose choice for remeshing applications (see e.g. Figure 19). However, this choice can also lead to a sub-optimal mapping for highly

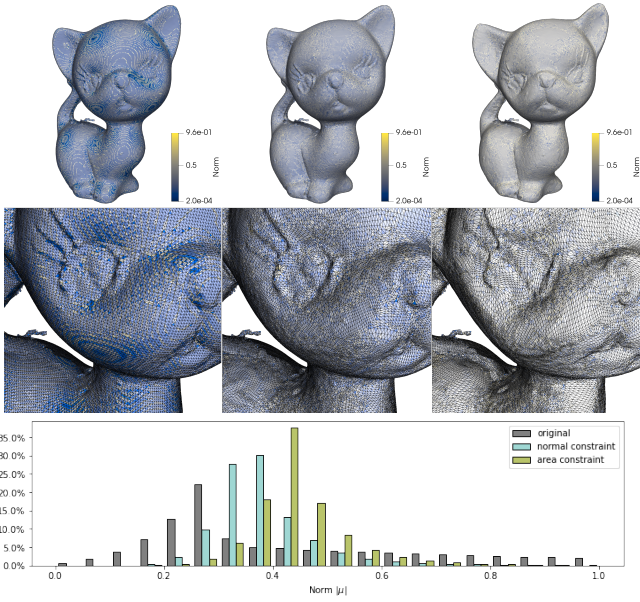


Fig. 19. QC remeshings of a kitten mesh (colored by  $|\mu|$ ) with genus one and 19 boundary components constructed using the QC Iteration algorithm from Section 5 with respect to an equi-angular conformal structure. Left: original surface; Middle: remeshing with normal constraint (c.f. Section 4.1). Right: remeshing with area constraint (c.f. Section 4.2). Bottom: histogram of  $|\mu|$ .

irregular meshes, as vertices of the surface  $M_h$  may lie on a variable number of elements. In this case, it can be more beneficial to use the “optimized” Algorithm 5 to determine shape of each reference element. This procedure chooses interior angles in such a way that the largest angle of each element dominates the choice of conformal structure. To describe this in more detail, consider that any vertex  $v_i$  away from the boundary is surrounded by a fixed number of elements  $m_i$ , and for each element containing  $v_i$  it is desirable for the corresponding interior angle  $\alpha_i$  to be as close as possible to  $2\pi/m_i$ . Moreover, the sum of the interior angles  $\alpha_i$  in each element should equal  $\pi$  or  $2\pi$  for triangular or quadrilateral elements, respectively. Therefore, if a leading vertex  $v_i$  exists in an element such that  $\alpha_i > \alpha_j$  for all  $j \neq i$ , Algorithm 5 fixes  $\alpha_i$  and redistributes the remaining exterior angle sum  $\pi - \alpha_i$  (or  $2\pi - \alpha_i$  for quadrilateral elements) to the other vertices  $v_j$  proportionally to the value of  $\alpha_j$ . If a leading vertex does not exist in a particular element, then the exterior angle sum  $\pi$  (or  $2\pi$  for quadrilateral elements) is instead redistributed to all vertices  $v_j$  proportionally to the value of  $\alpha_j$ . This provides a heuristic choice of conformal structure [ $g_{ref}$ ] which leads to qualitatively different behavior than the equi-angular choice described before. An illustration of this can be seen in Figure 20, where changing the conformal structure corresponding to  $g_{ref}$  yields a noticeable change in the results. Unsurprisingly, a more dilatation-uniform result in this case is obtained by using the conformal structure coming from Algorithm 5 which is adapted to the source surface.

**Remark 6.1.** Because the target mesh is implicit, the use of a user-defined reference metric  $g_{ref}$  makes the result of Algorithm 1 (and hence Algorithm 2) somewhat independent of the conformal structure on the source surface  $M \subset \mathbb{R}^3$  induced by its embedding. This is highly useful in many cases; since computational meshes often contain elements which are nearly degenerate (e.g. Figures 1 and 19), it is desirable to have algorithms which do not depend strongly on mesh quality. On the other hand, the results of these procedures will still be influenced by the combinatorics of the original mesh, since Algorithm 5 still makes use of connectivity information.

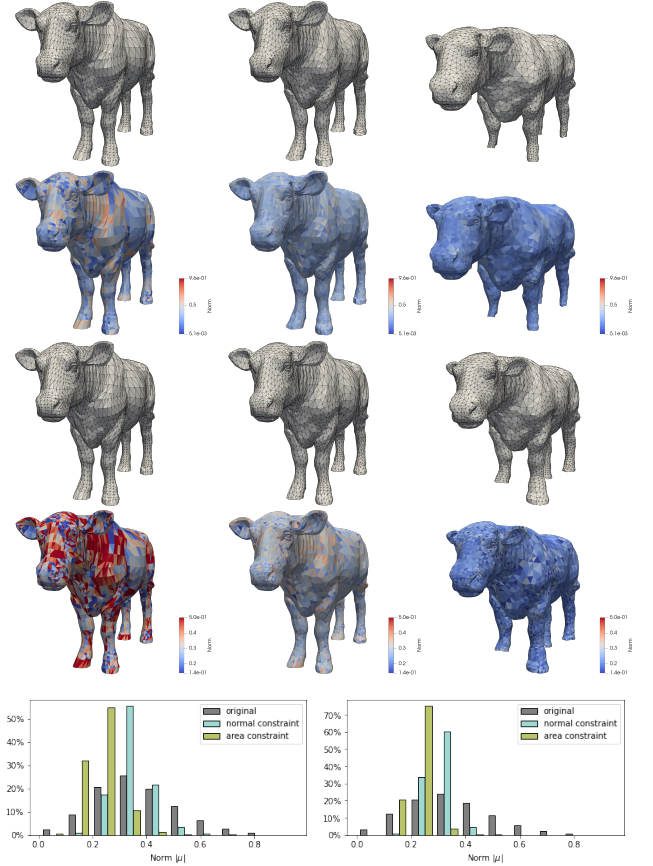


Fig. 20. Top two rows: equi-angular conformal structure; original surface (left), TQCM with normal constraint (middle), TQCM with area constraint (right). Next two rows: same as above but with conformal structure found by Algorithm 5. Bottom row: histogram corresponding to top two rows (left), histogram corresponding to next two rows (right).

This Section is finished with some specific discussion of the remeshing examples displayed here. Figure 18 illustrates how the constraints on area and extrinsic geometry from Section 4 can be used along with the QC Iteration to produce optimal quasiconformal maps which respect sharp features such as corners in the original mesh. Notice that there is a trade-off observed between conformal distortion and geometry preservation; the rounder area-constrained

mapping has a norm  $|\mu|$  which is significantly left-shifted compared to the sharper normal-constrained mapping. Perhaps this is also related to the fact that minimizing  $QC_\mu$  is equivalent to minimizing the Dirichlet energy  $\mathcal{D}_g(\mu)$  when the area is fixed. A similar comparison is carried out in Figure 19, which represents a more challenging example for Algorithm 2. Again, the original mesh is greatly improved on average (although not quite dilatation-uniform), and the constraints have a noticeable effect on the optimal mapping. Interestingly, here the area-constrained mapping is both more heavily distorted and more dilatation-uniform than its normal-constrained equivalent. The final remeshing example presented here is Figure 21, which shows that optimal quasiconformal mappings may or may not be preferred over least-squares conformal mapping procedures when high-quality LSCMs can be produced. In this case, a double torus with constrained area is remeshed using both Algorithm 2 and Algorithm 1 with  $\mu = 0$  (i.e. least-squares conformal mapping). Notice that the LSCM produces a very low-distortion mapping at the cost of uniformity in  $|\mu|$ , while the result of QC Iteration is highly uniform but more distorted. Therefore, the decision of which remeshing technique is most advantageous for any given application is ultimately the choice of the practitioner.

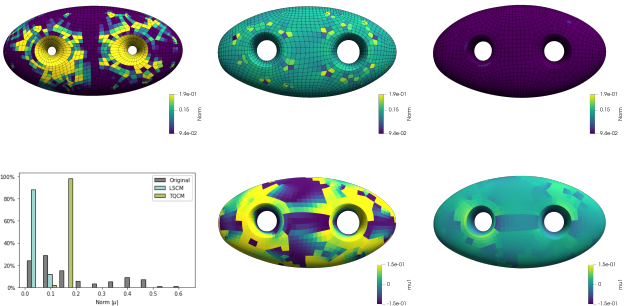


Fig. 21. A comparison of optimal quasiconformal remeshing procedures when area is constrained. Top row: least-squares conformal mapping (top right) and QC Iteration (top middle) on a double torus (top left), colored by  $|\mu|$  and with respect to the conformal structure given by Algorithm 5. Bottom row: histogram, plots of  $\mu^1$  for the surfaces above. Notice that the LSCM produces less distortion at the cost of uniformity in the mapping.

## 7 CONCLUSIONS AND FUTURE WORK

A quaternionic representation of quasiconformal mappings whose domain is an immersed surface in  $\mathbb{R}^3$  has been introduced, and a least-squares algorithm for computing these objects has been discussed. When the Beltrami coefficient  $\mu$  is known, this procedure requires only the solution of a linear system and reconstructs the quasiconformal mapping which best represents  $\mu$  in the homotopy class of the given initial data. This has enabled a quaternionic version of the QC Iteration Algorithm from [Lui et al. 2015, 2014], which computes optimal Teichmüller mappings in the case of simply connected surfaces and dilatation-uniform quasiconformal mappings otherwise. The present QC Iteration is applicable to both planar and non-planar manifold meshes and is amenable to optional constraints

on surface area and extrinsic geometry. Illustrative examples have demonstrated the utility of these algorithms for object deformation and surface remeshing applications.

Despite the advances discussed here, there remain several challenges and avenues for future work in this area. For one, there is still no satisfactory algorithm for computing Teichmüller extremal mappings between Riemann surfaces of arbitrary genus. Since it has been proven (see [Lui et al. 2015]) that these mappings can be computed by an iterative procedure such as the QC Iteration in many cases of interest, it remains important to find a rigorous alternative to the heuristic Step 3 of this procedure which is guaranteed to always make progress toward the unique extremal mapping. On the other hand, it would be even more useful to have a direct, single-stage minimization algorithm which computes the optimal Teichmüller mapping given an initial surface, boundary data, and homotopy class. Finally, it should be mentioned that nearly every treatment of computational quasiconformal mapping to date relies on solving a discretized problem which agrees with the smooth theory only in the limit of mesh refinement. It would be highly interesting to see progress toward a fully discrete theory for quasiconformality similar to what is currently being developed for conformality.

## ACKNOWLEDGMENTS

The original meshes in Figures 1, 11, 18, 19, and 20 are provided courtesy of the AIM@SHAPE repository, and the original mesh in Figure 6 is provided courtesy of Keenan Crane. The dot texture is courtesy of www.pixabay.com and the checkerboard texture is courtesy of www.textures.com. The research of the second author was partially supported by the NSF grant DMS-1912902.

## REFERENCES

- E Aulisa, S Bna, and G Bornia. 2014. FEMuS Finite Element Multiphysics Solver. *Github repository* (2014).
- Alexander I Bobenko, Ulrich Pinkall, and Boris A Springborn. 2015. Discrete conformal maps and ideal hyperbolic polyhedra. *Geometry & Topology* 19, 4 (2015), 2155–2215.
- Francis E Burstall, Dirk Ferus, Katrin Leschke, Franz Pedit, and Ulrich Pinkall. 2004. *Conformal geometry of surfaces in  $S^4$  and quaternions*. Springer.
- Gary Choi. 2021. Efficient conformal parameterization of multiply-connected surfaces using quasi-conformal theory. *J. Sci. Comput.* 87, 3 (2021), 1–19.
- Gary PT Choi, Hei Long Chan, Robin Yong, Sarbin Ranjikar, Alan Brook, Grant Townsend, Ke Chen, and Lok Ming Lui. 2020. Tooth morphometry using quasi-conformal theory. *Pattern Recognition* 99 (2020), 107064.
- Georgios Daskalopoulos and Richard A Wentworth. 2007. Harmonic maps and Teichmüller theory. *Handbook of Teichmüller theory* 1 (2007), 33–109.
- Gerhard Dziuk and Charles M Elliott. 2013. Finite element methods for surface PDEs. *Acta Numerica* 22 (2013), 289.
- James Eells and Joseph H Sampson. 1964. Harmonic mappings of Riemannian manifolds. *American journal of mathematics* 86, 1 (1964), 109–160.
- Frederick P Gardiner. 1987. Teichmüller theory and quadratic differentials. *Pure Appl. Math.* (1987).
- Frederick P Gardiner and Nikola Lakic. 2000. Quasiconformal Teichmüller Theory. (2000).
- Anthony Gruber and Eugenio Aulisa. 2020. Computational P-Willmore Flow with Conformal Penalty. *ACM Trans. Graph.* 39, 5, Article 161 (Aug. 2020), 16 pages. <https://doi.org/10.1145/3369387>
- Xianfeng Gu, Yalin Wang, Tony F Chan, Paul M Thompson, and Shing-Tung Yau. 2004. Genus zero surface conformal mapping and its application to brain surface mapping. *IEEE transactions on medical imaging* 23, 8 (2004), 949–958.
- Xianfeng Gu and Shing-Tung Yau. 2003. Global Conformal Surface Parameterization. In *Proceedings of the 2003 Eurographics/ACM SIGGRAPH Symposium on Geometry Processing (SGP ’03)*. Eurographics Association, 127–137.
- Kin Tat Ho and Lok Ming Lui. 2016. QCMC: quasi-conformal parameterizations for multiply-connected domains. *Advances in Computational Mathematics* 42, 2 (2016), 279–312.

- JH Hubbard. 2006. Teichmüller Theory and Applications to Geometry, Topology and Dynamics, Volume I: Teichmüller Theory. (2006).
- George Kamberov, Franz Pedit, and Peter Norman. 2002. *Quaternions, spinors, and surfaces*. American Mathematical Society.
- Liliya Kharevych, Boris Springborn, and Peter Schröder. 2006. Discrete Conformal Mappings via Circle Patterns. *ACM Trans. Graph.* 25, 2 (April 2006), 412–438. <https://doi.org/10.1145/1138450.1138461>
- Yin Tat Lee, Ka Chun Lam, and Lok Ming Lui. 2016. Landmark-matching transformation with large deformation via n-dimensional quasi-conformal maps. *Journal of Scientific Computing* 67, 3 (2016), 926–954.
- B. Lévy, S. Petitjean, N. Ray, and J. Maillot. 2002. Least squares conformal maps for automatic texture atlas generation. In *ACM transactions on graphics (TOG)*, Vol. 21. ACM, 362–371.
- Yaron Lipman. 2012. Bounded Distortion Mapping Spaces for Triangular Meshes. *ACM Trans. Graph.* 31, 4, Article 108 (July 2012), 13 pages.
- Lok Ming Lui, Xianfeng Gu, and Shing-Tung Yau. 2015. Convergence of an iterative algorithm for Teichmüller maps via harmonic energy optimization. *Math. Comp.* 84, 296 (2015), 2823–2842.
- Lok Ming Lui, Ka Chun Lam, Shing-Tung Yau, and Xianfeng Gu. 2014. Teichmüller mapping (t-map) and its applications to landmark matching registration. *SIAM Journal on Imaging Sciences* 7, 1 (2014), 391–426.
- Ting Wei Meng, Gary Pui-Tung Choi, and Lok Ming Lui. 2016. TEMPO: Feature-Endowed Teichmüller Extremal Mappings of Point Clouds. *SIAM Journal on Imaging Sciences* 9, 4 (2016), 1922–1962. <https://doi.org/10.1137/15m1049117>
- TC Ng, Xianfeng Gu, and LM Lui. 2014. Teichmüller extremal map of multiply-connected domains using Beltrami holomorphic flow. *Journal of Scientific Computing* 60, 2 (2014), 249–275.
- Xianshu Nian and Falai Chen. 2016. Planar domain parameterization for isogeometric analysis based on Teichmüller mapping. *Computer Methods in Applied Mechanics and Engineering* 311 (2016), 41–55.
- Jing Peng, Douglas R Heisterkamp, and Ho Kwok Dai. 2004. Adaptive quasiconformal kernel nearest neighbor classification. *IEEE Transactions on Pattern Analysis and Machine Intelligence* 26, 5 (2004), 656–661.
- Ulrich Pinkall and Konrad Polthier. 1993. Computing discrete minimal surfaces and their conjugates. *Experimental mathematics* 2, 1 (1993), 15–36.
- Di Qiu, Ka-Chun Lam, and Lok-Ming Lui. 2019. Computing Quasi-Conformal Folds. *SIAM Journal on Imaging Sciences* 12, 3 (2019), 1392–1424.
- Rohan Sawhney and Keenan Crane. 2017. Boundary First Flattening. *ACM Trans. Graph.* 37, 1, Article 5 (Dec. 2017), 14 pages. <https://doi.org/10.1145/3132705>
- Boris Schäling. 2011. *The boost C++ libraries*. Boris Schäling.
- Boris Springborn, Peter Schröder, and Ulrich Pinkall. 2008. Conformal Equivalence of Triangle Meshes. *ACM Trans. Graph.* 27, 3 (Aug. 2008), 1–11. <https://doi.org/10.1145/1360612.1360676>
- Kurt Strebel. 1978. On quasiconformal mappings of open Riemann surfaces. *Commentarii Mathematici Helvetici* 53, 1 (1978), 301–321.
- Kurt Strebel. 1984. Quadratic differentials. In *Quadratic Differentials*. Springer, 16–26.
- Lloyd N Trefethen. 2020. Numerical conformal mapping with rational functions. *Computational Methods and Function Theory* 20, 3 (2020), 369–387.
- Ofir Weber, Ashish Myles, and Denis Zorin. 2012. Computing extremal quasiconformal maps. In *Computer Graphics Forum*, Vol. 31. Wiley Online Library, 1679–1689.
- Jinlan Xu, Hongmei Kang, and Falai Chen. 2018. Content-aware image resizing using quasi-conformal mapping. *The Visual Computer* 34, 3 (2018), 431–442.
- Yi-Jun Yang and Wei Zeng. 2020. Quasiconformal rectilinear map. *Graphical Models* 107 (January 2020), 101057. <https://doi.org/10.1016/j.gmod.2019.101057>
- Wei Zeng and Xianfeng David Gu. 2011. Registration for 3D surfaces with large deformations using quasi-conformal curvature flow. In *CVPR 2011*. IEEE, 2457–2464.
- Wei Zeng, Lok Ming Lui, Feng Luo, Tony Fan-Cheong Chan, Shing-Tung Yau, and David Xianfeng Gu. 2012. Computing quasiconformal maps using an auxiliary metric and discrete curvature flow. *Numer. Math.* 121, 4 (2012), 671–703.

## A HARMONIC VS TEICHMÜLLER

This Appendix gives a brief description of the connection between Teichmüller and harmonic maps which may be useful for understanding some results in the body. First, let  $f : M \rightarrow \mathbb{R}^3$  be a conformal immersion with normal  $N$ . Then, the area form is the trace of the metric tensor  $f^*\delta = |df|^2$ , since

$$\begin{aligned} \frac{N}{2} df \wedge \overline{df} &= -\frac{N}{2} (df * df - *df df) \\ &= -\frac{N}{2} (df N df - N df df) = |df|^2. \end{aligned}$$

On the other hand, the Dirichlet energy with respect to the metric  $g = f^*\delta$  also has the simplified expression,

$$\begin{aligned} \mathcal{D}_g(f) &= \frac{1}{2} \int_M df \wedge *df = \frac{1}{2} \int_M |df|^2 + |*df|^2 \\ &= \int_M |df|^2 = \mathcal{A}(f), \end{aligned}$$

so that  $\mathcal{D}_g = \mathcal{A}$  when  $f$  is conformal, and minimizing the Dirichlet energy is equivalent to minimizing the surface area. More generically, suppose  $f : M \rightarrow \mathbb{R}^3$  is a mapping which is not conformal, but there is a conformal structure on  $M$  specified by some other reference immersion (say  $z$ ) satisfying  $*dz = N dz$ . In this case,  $df = df^+ + df^-$  relative to this structure and the area form becomes

$$\begin{aligned} \frac{N}{2} df \wedge \overline{df} &= -\frac{N}{2} (df^+ \wedge df^+ + df^- \wedge df^- + df^+ \wedge df^- + df^- \wedge df^+) \\ &= |df^+|^2 - |df^-|^2, \end{aligned}$$

where it was used that

$$df^+ \wedge df^- = -\overline{df^- \wedge df^+} = df^+ * df^- - *df^+ df^- = 0.$$

In this case, the Dirichlet energy is

$$\mathcal{D}_g(f) = \frac{1}{2} \int_M df \wedge *df = \int_M |df^+|^2 + |df^-|^2,$$

which follows because

$$df^- \wedge *df^+ = df^+ \wedge *df^- = 0.$$

This gives a more general decomposition

$$\mathcal{D}_g(f) = \int_M |df^+|^2 - |df^-|^2 + 2 \int_M |df^-|^2 = \mathcal{A}(f) + 2C\mathcal{D}(f),$$

where  $\mathcal{A}$  is signed area and  $C\mathcal{D}$  is conformal distortion. Note that  $\mathcal{D}_g$  depends only on the metric  $\delta$  of  $\mathbb{R}^3$  and the conformal class of  $g$ , and that  $f$  is conformal if and only if  $C\mathcal{D}(f) = 0$ , in which case this expression reduces to the one above. Moreover, when the target of  $f$  is fixed, the area term does not vary and so the minimizers of  $C\mathcal{D}$  and  $\mathcal{D}_g$  are identical. This implies that any conformal map is also harmonic, which has proven to be quite useful for computing minimal surfaces and least-squares conformal mappings (see e.g. [Gruber and Aulisa 2020; Lévy et al. 2002; Pinkall and Polthier 1993]).

It turns out that a similar decomposition is quite useful for understanding Teichmüller quasiconformal mappings. Write  $g = \sigma |dz|^2$  for some local conformal coordinate  $z : U \subset M \rightarrow \mathbb{C}$  and recall that the quasiconformal distortion of the mapping  $f : M \rightarrow \mathbb{R}^3$  with Beltrami coefficient  $\mu : TM \rightarrow (TM)^\perp$  (c.f. Definition 3.3) is

$$\begin{aligned} 4QC_\mu(h) &:= 2 \int_M |dh^- - \mu dh^+|^2 dS_g \\ &= \int_U \frac{1}{\sigma} |\mathbf{h}_{\bar{z}} - \mu \mathbf{h}_z|^2 \sigma idz \wedge d\bar{z} = \int_U |\mathbf{h}_{\bar{z}} - \mu \mathbf{h}_z|^2 idz \wedge d\bar{z}, \end{aligned}$$

where we have abused notation by equating the global object  $QC_\mu$  with its representation on  $U$ . Since  $QC_\mu$  measures deviation from quasiconformality, it is natural to wonder if it appears as the conformal part of some Dirichlet energy functional. To examine this, recall that any mapping  $f : (M, g) \rightarrow f(M) \subset (\mathbb{R}^3, \delta)$  which is quasiconformal with respect to  $\mu$  induces a new metric on  $M$ , expressed locally as  $g(\mu) := f^*\delta = \rho |d\zeta|^2$ , where  $\rho = |\mathbf{f}_z|^2$  and  $d\zeta = dz + \mu d\bar{z}$ . This is simply the image metric expressed on the source surface  $M$ ,

which is not conformal to  $g$  unless  $\mu \equiv 0$ . There is then the usual notion of Dirichlet energy with respect to  $g(\mu)$ , expressed locally as

$$\begin{aligned} 2\mathcal{D}_{g(\mu)}(f) &= \int_M |df|^2 dS_{g(\mu)} = \int_U \frac{1}{\rho} \left( |\mathbf{f}_\zeta|^2 + |\mathbf{f}_{\bar{\zeta}}|^2 \right) \rho id\zeta \wedge d\bar{\zeta} \\ &= \int_U \left( |\mathbf{f}_\zeta|^2 + |\mathbf{f}_{\bar{\zeta}}|^2 \right) id\zeta \wedge d\bar{\zeta}, \end{aligned}$$

which depends on the metric  $\delta$  and the conformal class of  $g(\mu)$ . The next result (essentially due to [Lui et al. 2015, Lemma 3.3]) establishes a decomposition similar to that discussed earlier, which connects the critical points of  $\mathcal{D}_{g(\mu)}$  to those of  $QC_\mu$  in the case that  $\mu$  has constant norm.

**THEOREM A.1.** *Let  $\mu : TM \rightarrow TM$  be a Beltrami differential with constant norm  $|\mu| < 1$  corresponding to a quasiconformal map  $f : M \rightarrow f(M) \subset \mathbb{R}^3$ . Then, the Dirichlet energy  $\mathcal{D}_{g(\mu)}(h)$  of any mapping  $h : M \rightarrow \mathbb{R}^3$  decomposes as*

$$\mathcal{D}_{g(\mu)}(h) = \frac{2}{1 - |\mu|^2} QC_\mu(h) + \mathcal{A}(h).$$

In particular, when the area of the image is fixed, quasiconformal maps with BC  $\mu$  are also harmonic with respect to the metric  $g(\mu)$ .

**PROOF.** Consider local coordinates  $z, \zeta$  as above so that  $g = \sigma |dz|^2$ ,  $g(\mu) = \rho |d\zeta|^2 = |\mathbf{f}_\zeta|^2 |dz + \mu d\bar{z}|^2$ . A straightforward computation establishes the Jacobian determinants

$$\begin{aligned} id\zeta \wedge d\bar{\zeta} &= \left( |\zeta_z|^2 - |\zeta_{\bar{z}}|^2 \right) idz \wedge d\bar{z} = \left( 1 - |\mu|^2 \right) idz \wedge d\bar{z}, \\ dh \wedge d\bar{h} &= \left( |\mathbf{h}_\zeta|^2 - |\mathbf{h}_{\bar{\zeta}}|^2 \right) id\zeta \wedge d\bar{\zeta}, \end{aligned}$$

and using the representations of  $d\zeta, d\bar{\zeta}$  in terms of  $dz, d\bar{z}$  leads to the partial derivatives

$$\mathbf{h}_\zeta = \frac{1}{1 - |\mu|^2} (\mathbf{h}_z - \bar{\mu} \mathbf{h}_{\bar{z}}), \quad \mathbf{h}_{\bar{\zeta}} = \frac{1}{1 - |\mu|^2} (\mathbf{h}_{\bar{z}} - \mu \mathbf{h}_z).$$

Therefore, when  $\mu$  has constant norm, the energy  $\mathcal{D}_{g(\mu)}$  may be expressed as

$$\begin{aligned} 2\mathcal{D}_{g(\mu)}(h) &= \int_U 2|\mathbf{h}_\zeta|^2 id\zeta \wedge d\bar{\zeta} + \int_U \left( |\mathbf{h}_\zeta|^2 - |\mathbf{h}_{\bar{\zeta}}|^2 \right) id\zeta \wedge d\bar{\zeta} \\ &= \frac{2}{1 - |\mu|^2} \int_U |\mathbf{h}_z - \bar{\mu} \mathbf{h}_{\bar{z}}|^2 idz \wedge d\bar{z} + \int_U dh \wedge d\bar{h} \\ &= \frac{4}{1 - |\mu|^2} QC_\mu(h) + 2\mathcal{A}(h), \end{aligned}$$

where  $\mathcal{A}(h)$  is the signed area of the image surface, counted with multiplicity. Therefore, when this area is fixed  $\mathcal{D}_{g(\mu)}$  and  $QC_\mu$  have the same set of critical points.  $\square$

Since Teichmüller mappings are unique when they exist and correspond to Beltrami coefficients with constant norm, Theorem A.1 implies that any homotopy class of maps from  $M$  into a fixed target which contains a Teichmüller extremum corresponding to the BC  $\mu^*$  also contains a unique harmonic map with respect to the conformal class of  $g(\mu^*)$ , and that these maps actually coincide. Conversely, in this case it follows that minimizing  $QC_\mu$  for a constant-norm  $\mu$  is equivalent to minimizing the Dirichlet energy  $\mathcal{D}_{g(\mu)}$ . These facts are what underlie the QC Iteration algorithm, and may explain

why the mappings with fixed area computed through this process generally have more optimal distortion profiles (see e.g. Figures 1, 18, and 19).

## B THEORY OF QC ITERATION

This Appendix recalls some theory from [Lui et al. 2015] which is useful for understanding the QC Iteration algorithm. Precisely, the QC Iteration involves an energy functional on the space of Beltrami differentials  $\mu$  associated to quasiconformal mappings  $f : M \rightarrow P$  between fixed Riemann surfaces, denoted  $\mathcal{B}(M, P)$ . To describe this object, first recall that a local conformal coordinate  $z : U \subset M \rightarrow \mathbb{C}$  on the Riemann surface  $(M, J)$  gives rise to a conformal class of Riemannian metrics  $[g] = \{g_\sigma = \sigma |dz|^2 \mid \sigma : U \rightarrow \mathbb{R}^+\}$  compatible with  $J$ , and that any quasiconformal mapping  $f : (M, g) \rightarrow (P, h)$  ( $h$  a metric compatible with the complex structure on  $P$ ) with BC  $\mu$  gives rise to a similar conformal class  $[g(\mu)]$  containing  $\sigma$ -multiples of the canonical representative  $g(\mu) = |dz + \mu d\bar{z}|^2$ . Under certain assumptions including compact  $P$  with nonpositive Gaussian curvature (see e.g. [Eells and Sampson 1964, Section 11]), it follows that there is a unique harmonic mapping  $f^* : (M, g(\mu)) \rightarrow (P, h)$  in the homotopy class  $[f]$  which depends only on the metric  $h$  and the conformal class of  $g(\mu)$ .

This suggests a definition for the *Beltrami energy* of the BC  $\mu$ ,

$$\mathcal{E}(\mu) := \mathcal{D}_{g(\mu)}(f^*) = \frac{1}{2} \int_M |df^*|_h^2 dS_{g(\mu)},$$

where  $f^* = f^*(\mu, h)$ ,  $dS_{g(\mu)}$  and  $\mathcal{D}_{g(\mu)}$  denote respectively the area element and Dirichlet energy with respect to the metric  $g(\mu)$ , and  $|\cdot|_h$  denotes the norm with respect to the metric  $h$ . Under assumptions such as those of Theorem 2.2, it can be shown (see [Lui et al. 2015, Theorem 3.2]) that  $\mathcal{E}$  has a unique global minimizer in each “conformal class” of Beltrami differentials  $[\mu]$ , where  $\mu' \sim \mu$  if there is a biholomorphism  $(M, g(\mu')) \mapsto (M, g(\mu))$  homotopic to the identity map. Therefore, when a unique Teichmüller map  $f^{**} : M \rightarrow P$  exists for some  $[f]$ , the Beltrami energy  $\mathcal{E}$  has a global minimizer which is precisely the associated BC  $\mu^{**}$ . Moreover, it follows that  $f^{**} : (M, g(\mu^{**})) \rightarrow (P, h)$  is a conformal mapping.

With this, the QC Iteration can be understood as an iterative procedure which computes the Teichmüller mapping  $f^{**} \in [f]$  by following a sequence of Beltrami differentials  $\{\mu^*\}$  corresponding to unique harmonic maps  $f^* : (M, g(\mu)) \rightarrow (P, h)$ . Ideally, the minimum should be produced by performing gradient descent on  $\mathcal{E}$ , although this is generally difficult. Instead, the authors of [Lui et al. 2014] formulate the heuristic Step 3 discussed at length in Section 5.3 which often (but not always) decreases the Beltrami energy. It would be interesting to find a rigorous way to ensure that the motion of  $\mu$  is not orthogonal to  $\nabla \mathcal{E}$ , so that the desired extremal mapping is better approximated in all cases of interest.

## C PROOF OF LEMMA 2.4

Recall that in the local conformal coordinate  $z : U \subset M \rightarrow \mathbb{C}$  the Teichmüller Beltrami coefficient satisfies

$$\mu = k \frac{\bar{q}}{|q|},$$

where  $k \in \mathbb{R}$  and  $q : U \rightarrow \mathbb{C}$  is a local holomorphic function. It follows immediately that the norm is constant, hence harmonic.

Moreover, since  $q$  is holomorphic, so is  $\log q = \log |q| + i \arg q$  (in an appropriate branch) and it follows that  $\arg q$  is harmonic. Finally, we have the phase equality

$$e^{i \arg \mu} = \frac{\bar{q}}{|q|},$$

so that  $\arg \mu = -\arg q$ , which implies the first conclusion. Conversely, if  $\theta : U \rightarrow \mathbb{R}$  is a harmonic function, then there is a conjugate harmonic function  $\phi$  so that  $\phi - i\theta$  is holomorphic. In this case,  $q = e^{\phi - i\theta}$  is also holomorphic and

$$\mu = |\mu| e^{i\theta} = k \frac{\bar{q}}{|q|}$$

is Teichmüller.

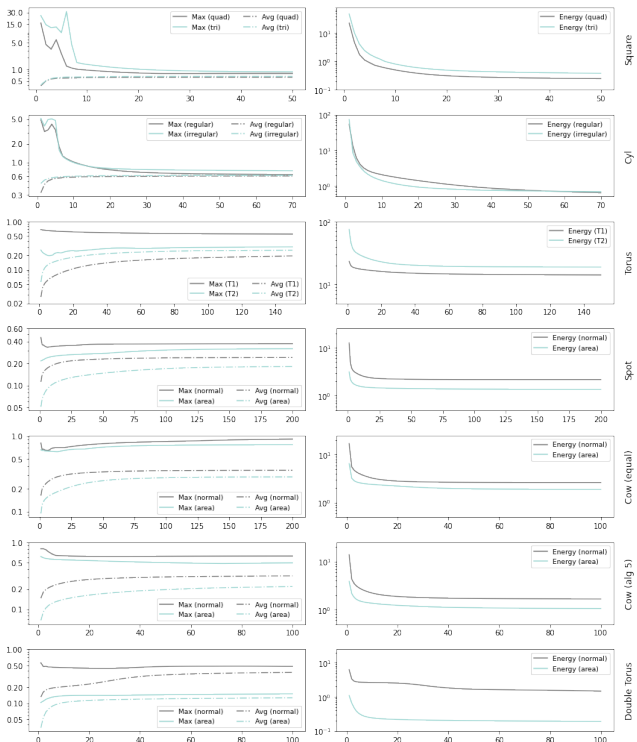


Fig. 22. Quantitative plots corresponding to a representative cross-section of experiments from the body. The left column displays  $|\mu|_\infty$  along with  $|\mu|_{\text{avg}}$  at the end of each iteration, which ideally become near-equal. The right column displays the quasiconformal distortion  $QC_\mu(f)$  at the end of each iteration; note that the line search in Section 5.4 forces this quantity to be nonincreasing.

## D DEPENDENCE ON DISCRETIZATION AND CONSTRAINTS

This Appendix takes a deeper look into the discretization- and constraint- dependence of Algorithms 1 and 2. Given prescribed Dirichlet boundary data, Figure 23 displays the result of computing an extremal Teichmüller mapping from a square discretized three different ways to the corresponding planar domain realizing this

boundary. In all cases, the mappings are computed with respect to an ideal equi-angular conformal structure on the domain, so that both quad meshes produce the same mapping as their combinatorics are identical. On the other hand, the triangular mesh produces a mapping which is essentially different from the others; a pole appears in the lower-left corner of the domain which is not present in the quad-meshed cases. Note that all mappings have highly uniform conformativity distortion, although the distortion of the triangular domain is slightly higher.

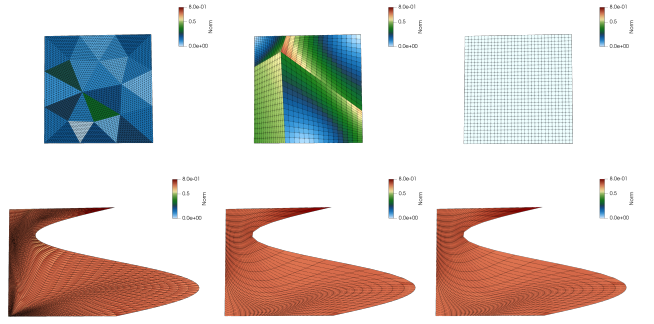


Fig. 23. A comparison between the Teichmüller maps generated by Algorithm 2 for three different discretizations of the square domain for the same boundary data, colored by  $|\mu|$  in the left and middle columns and by  $\mu^1$  in the right column. Note that all are mappings are computed with respect to an equi-angular conformal structure on the domain. As a consequence, the middle and right mappings are identical.

The results of a similar experiment carried out for a non-planar case are given in Figure 24. Here, the cylindrical domain from Figure 5 is sheared according to a closed curve on the surface and discretized accordingly, so that its inherited conformal structure is different from the meshing with regular squares. In this case, Algorithm 5 produces different reference conformal structures based on these discretizations, which leads to different mappings computed by Algorithm 2 to the surface with prescribed boundary data. Notice that aspects such as the location of the zero and pole of the associated quadratic differential are dependent on this discretization, since they depend on the conformal structure of the domain. Similarly, the optimal distortion  $|\mu|$  is different as well.

In addition to the pictorial information seen thusfar, Figure 22 displays plots of various quantities corresponding to a representative cross-section of experiments from the body. Particularly, the average and maximum norms of the BC  $\mu$  are displayed at each iteration, which should tend to each other in the case that a Teichmüller mapping is arbitrarily approximated by Algorithm 2. Moreover, the quasiconformal distortion  $QC_{\mu_{k+1}}(f_k)$  at the end of each iteration is also reported, to give an idea of its decrease and eventual plateau. The first row of Figure 22 compares the mappings involving the regular quad mesh of the square and the triangular mesh from Figure 23, row 2 compares the mappings from Figure 24, row 3 compares the mappings from Figure 16, row 4 compares the mapping from Figure 6 computed using the normal constraint from Section 4.1 to another mapping (not pictured) computed using the area constraint

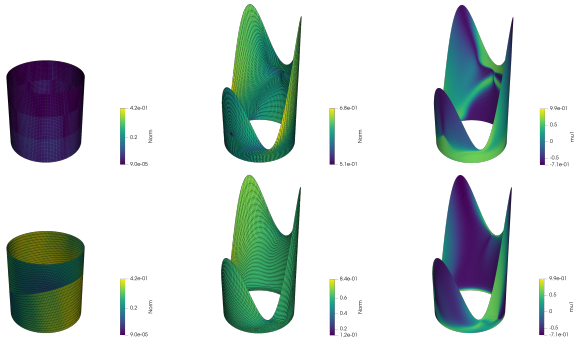


Fig. 24. A comparison of the extremal mappings generated by Algorithm 2 for two different discretizations of the round cylinder with reference conformal structures computed by Algorithm 5. Note the different locations of the discontinuities in  $\mu$ .

Section 4.2, rows 5 and 6 compare the mappings from 20, and row 7 compares the optimal quasiconformal mapping from Figure 21 computed using the area constraint to another mapping (not pictured) computed using the normal constraint. Notice that the QC Iteration Algorithm 2 finds optimal Teichmüller mappings with varying success; extremal mappings involving genus zero surfaces with boundary are very well approximated, while remeshings such as that displayed in Figure 20 remain relatively far from the Teichmüller criterion. This could be due in large part to the lack of an appropriate conformal structure on the domain, as suggested by the smaller difference between the maximum and average values of  $|\mu|$  when the conformal structure is pre-computed through Algorithm 5. It is further remarkable that in a typical instance of remeshing with Algorithm 2 there are often only a handful elements which realize the maximum conformality distortion, with the rest lying close to the average.